MECHANISMS GENERATING CANCER GENOME COMPLEXITY FROM A SINGLE CELL DIVISION ERROR

Neil T. Umbreit[1,2,3,*,†], Cheng-Zhong Zhang[4,5,*,†], Luke D. Lynch[2,3], Logan J. Blaine[2,3], Anna M. Cheng[1,2,3], Richard Tourdot[4,5], Lili Sun[8], Hannah F. Almubarak[4,5], Kim Judge[6], Thomas J. Mitchell[6,7], Alexander Spektor[2,3,9], and David Pellman[1,2,3,†]

Author Affiliations

1. Howard Hughes Medical Institute, Chevy Chase, MD, USA
2. Department of Cell Biology, Harvard Medical School, Boston, MA, USA
3. Department of Pediatric Oncology, Dana-Farber Cancer Institute, Boston, MA, USA
4. Department of Biomedical Informatics, Harvard Medical School, Boston, MA, USA
5. Department of Data Sciences, Dana-Farber Cancer Institute, Boston, MA, USA
6. Wellcome Sanger Institute, Hinxton, Cambridgeshire, CB10 1SA, UK
7. Cambridge University Hospitals NHS Foundation Trust, Cambridge, CB2 0QQ, UK
8. Single-Cell Sequencing Program, Dana-Farber Cancer Institute, Boston, MA, USA
9. Department of Radiation Oncology, Dana-Farber Cancer Institute, Boston, MA, USA

*These authors contributed equally to this work

†Corresponding authors

Correspondence regarding biological experiments and requests for materials should be addressed to neilt_umbreit@dfci.harvard.edu and to david_pellman@dfci.harvard.edu

Correspondence regarding sequencing analysis and requests for sequencing data should be addressed to cheng-zhong_zhang@dfci.harvard.edu

22

ABSTRACT

24 The chromosome breakage-fusion-bridge (BFB) cycle is a mutational process that
25 produces gene amplification and genome instability. Signatures of BFB cycles can be observed in
26 cancer genomes with chromothripsis, another catastrophic mutational process. Here, we explain
27 this association by identifying a mutational cascade downstream of chromosome bridge formation
28 that generates increasing amounts of chromothripsis. We uncover a new role for actomyosin forces
29 in bridge breakage and mutagenesis. Chromothripsis then accumulates starting with aberrant
30 interphase replication of bridge DNA, followed by an unexpected burst of mitotic DNA
31 replication, generating extensive DNA damage. Bridge formation also disrupts the centromeric
32 epigenetic mark, leading to micronucleus formation that itself promotes chromothripsis. We show
33 that this mutational cascade generates the continuing evolution and sub-clonal heterogeneity
34 characteristic of many human cancers.

35

INTRODUCTION

37 Cancer genomes can contain thousands of chromosomal rearrangements (*1*).
38 Traditionally, it was assumed that these genomes evolve gradually by accruing small-scale
39 changes successively over many generations. However, the extent of genomic rearrangement in
40 many cancers suggests a non-exclusive, alternative view: these genomes may evolve rapidly via
41 discrete episodes that generate bursts of genomic alterations (*2-6*). This latter model provides a
42 parsimonious explanation for the origin of extreme genomic complexity.

43 Three classes of catastrophic events have been described that may account for a substantial
44 fraction of chromosome alterations in cancer: whole-genome duplication, chromothripsis, and

bioRxiv preprint doi: https://doi.org/10.1101/835058. this version posted November 7, 2019. The copyright holder for this preprint (which was not peer-reviewed) is the author/funder, who has granted bioRxiv a license to display the preprint in perpetuity. All rights reserved. No reuse allowed without permission.

chromosome breakage-fusion-bridge cycles. The first class, whole-genome duplication (WGD), can promote tumorigenesis and is now appreciated to occur during the development of ~40% of human solid tumors (*2, 7*). Whole-genome duplication causes genome instability by several mechanisms, including doubling the number of centrosomes, distorting spindle architecture, generating chromosome segregation errors, and producing micronuclei, abnormal nuclear structures common in cancer (*8-11*).

The second class of catastrophic event, chromothripsis, is a massive rearrangement of only one or a few chromosomes resulting in an unusual DNA copy number pattern (*3, 5, 12*). Chromothripsis occurs with reported frequencies of 20–65% in many common tumor types (*1, 13*). We previously found that chromothripsis can originate from micronuclei (*14-17*), which arise from mitotic segregation errors or unrepaired DNA breaks that generate acentric chromosome fragments. Due to aberrant nuclear envelope assembly around these chromosomes, micronuclei undergo defective DNA replication and spontaneous loss of nuclear envelope integrity, which results in extensive DNA damage by unknown mechanisms (*18, 19*).

The third class of catastrophic event, the chromosome breakage-fusion-bridge (BFB) cycle (*20, 21*), starts with cell division errors that trigger the formation of another abnormal nuclear structure, a chromosome bridge. Bridges arise from telomere crisis and end-to-end chromosome fusions but can also occur from end fusions at DNA breaks, incomplete DNA replication, or a failure to resolve chromosome catenation (*22*). Bridge breakage then initiates a process that can generate gene amplification after multiple cell generations. Evidence of BFB cycles has been reported in a broad range of cancer types, with estimated frequencies ranging up to ~80% in pancreatic cancer (*13*).

bioRxiv preprint doi: https://doi.org/10.1101/835058. this version posted November 7, 2019. The copyright holder for this preprint (which was not peer-reviewed) is the author/funder, who has granted bioRxiv a license to display the preprint in perpetuity. All rights reserved. No reuse allowed without permission.

Although BFB cycles are major sources of genome instability, the perfect palindromic sequence pattern expected from the originally proposed BFB model is not commonly observed in cancer genomes (*1, 13, 23*). Whether this is due to subsequent chromosomal rearrangement obscuring the simple BFB pattern, or whether the BFB process itself is inherently more complex than originally envisioned, has been unclear. Recently, comprehensive cancer genome sequencing has uncovered examples where signatures of the BFB cycle are intermingled with chromothripsis, raising the possibility that coupling of these two processes could add complexity to BFB cycles (*23*). However, to determine the relationship between BFB cycles and chromothripsis, it is first necessary to better understand the BFB cycle, for which many key mechanistic steps, particularly how chromosome bridges are broken, remain unclear.

Proposed models for chromosome bridge breakage have included breakage by spindle forces during the mitosis in which they are formed or DNA cleavage by the cytokinesis/abscission apparatus (*21, 24-26*). Yet recent work indicates that chromosome bridges are rarely, if ever, broken during mitosis or cytokinesis, but rather persist for many hours into interphase (*26, 27*). It was then proposed that interphase bridges are severed by the cytoplasmic, endoplasmic reticulum-associated exonuclease, TREX1 (*26*). Transient nuclear envelope (NE) disruption was suggested to allow TREX1 to enter the nucleus and gain access to the bridge DNA, simultaneously breaking the bridge and fragmenting the bridge DNA to generate chromothripsis (*26*). Although the TREX1-model could explain the association between BFB cycles and chromothripsis in cancer genomes (*23*), loss of TREX1 was reported to delay, but not block, bridge breakage (*26*).

Below, we present data supporting a new model that explains the linkage between BFB cycles and chromothripsis. Rather than being generated simultaneously by a single mechanism, we demonstrate that chromothripsis accumulates through a cascade of new mutational events

bioRxiv preprint doi: https://doi.org/10.1101/835058. this version posted November 7, 2019. The copyright holder for this preprint (which was not peer-reviewed) is the author/funder, who has granted bioRxiv a license to display the preprint in perpetuity. All rights reserved. No reuse allowed without permission.

initiated by the formation of a chromosome bridge. The first such event appears to involve defective DNA replication of bridge DNA, which, in a minority of cells, is associated with a newly-identified signature of DNA rearrangement in broken bridges during the interphase after bridge formation. Next, we observed extensive DNA damage and frequent chromothripsis associated with an unexpected burst of aberrant DNA replication on broken bridge "stubs" during the next mitosis. Then, because of compromised maintenance of the centromere epigenetic mark, CENP-A, the chromosomes with the broken bridge stubs mis-segregate with high frequency into micronuclei, which will generate further rounds of chromothripsis. Analysis of clonal populations after bridge breakage established that these events initiate iterative cycles of genome instability, causing extensive subclonal heterogeneity downstream of the formation of a single chromosome bridge. An analogous series of events was observed after the formation of micronuclei, indicating that similar mechanisms generate chromothripsis irrespective of the nuclear structure initiating the mutational cascade. Together, these findings reveal how a single cell division error rapidly generates extreme genomic complexity.

RESULTS

We used four methods to generate chromosome bridges to study their breakage and genomic impact: transient expression of a dominant negative variant of telomeric repeat-binding factor 2 (TRF2-DN) (*28*), partial knockdown of condensin (siSMC2) (*29*), low-dose topoisomerase II inhibition (ICRF-193) (*30*), and CRISPR/Cas9-mediated telomere loss on chromosome 4 (Chr4g1, Fig. S1A-C). TRF2-DN was employed to generate chromosome bridges in most experiments in this study, unless otherwise specified. Chromosome bridges were visualized in live cells with GFP-BAF (barrier-to-autointegration factor). GFP-BAF is a sensitive reporter for

these structures because, unlike histones (*26*), DNA binding by BAF is not compromised by the stretching of chromosome bridges during bridge extension (Fig. 1). For TRF2-DN, we developed transient expression and live-cell imaging conditions that avert the previously reported strong inhibition of cell cycle progression (*26*). In our conditions, cells with bridges entered S phase with similar timing after mitotic exit as unperturbed parental cells lacking bridges (8.3 versus 7.3 hr, respectively; Fig. S1D and accompanying legend). Importantly, bridges generated by each of the above four approaches all had similar lifetimes ($t_{1/2}$): ~10 hours from the completion of mitosis (Fig. 1A).

Mechanical force triggers chromosome bridge breakage

The cytoplasmic, endoplasmic reticulum-associated exonuclease, TREX1, has been suggested to mediate chromosome bridge breakage after rupture of the primary nucleus in bridged cells, as genetic ablation of TREX1 had a partial effect on bridge resolution (*26*). However, using the same cell lines and bridge induction method (and an additional method) but imaging conditions with less light exposure, we were unable to detect an effect of TREX1 knockout on bridge lifetime (six independent clones, two different knockout strategies, Fig. S2A-C). Additionally, a notable fraction of bridge breakage events occurred in the absence of any detectable rupture of the primary nucleus (36%, n = 58, Movie S1), and bridge lifetime showed no correlation with the occurrence or duration of nuclear envelope disruption (Fig. S2D). Therefore, fundamental aspects of the mechanism for bridge breakage remain to be identified.

A clue for alternative mechanisms comes from the fact that as interphase cells migrate in culture, bridges can reach hundreds of microns in length before breaking, raising the possibility that bridge breakage might have a mechanical component. Consistent with this idea, BJ foreskin fibroblasts, which exhibited similar motility to RPE-1 cells (cell velocity 0.48 and 0.51 μm/min,

136 respectively), extended and broke chromosome bridges during interphase with similar timing as
137 bridges in RPE-1 cells ($t_{1/2}$ = 7.4 hr; Fig. S3A and Movie S2). By contrast, two cell lines that
138 exhibited low motility (HeLa and U2OS) almost never extended bridges beyond 100 μm and rarely
139 underwent breakage before the next mitosis (10% and 20% interphase breakage, respectively; Fig.
140 S3B-C and Movies S3-4).

141 We hypothesized that the extension of chromosome bridges is required for their breakage.
142 To test this idea, we controlled bridge extension using rectangular fibronectin "micropatterns" that
143 constrain cell migration to the fibronectin-containing pattern (*31*). When RPE-1 cells were plated
144 on long (300 μm) patterns, newly formed chromosome bridges extended to ~160 μm on average,
145 and ~85% of bridges broke during interphase with similar kinetics as unconfined cells on glass
146 coverslips (Fig. 1B-C, Movie S5). By contrast, restricting bridge extension with short (100 μm)
147 micropatterns limited bridge extension to <50 μm and almost completely blocked bridge breakage
148 (<10% bridge cleavage prior to entry into the next mitosis; Fig. 1B-C, Movie S6). Although there
149 was less spontaneous NE rupture on short patterns, increasing NE ruptures >8-fold with Lamin B1
150 knockdown failed to accelerate bridge breakage on short patterns (Fig. S4). Therefore, the
151 extension of chromosome bridges, but not NE rupture, is required for their breakage.

152 Mechanical forces could stretch a bridge across its length or act locally within a section of
153 a bridge. Live-cell imaging supported the latter model: bridges often formed acute angle bends
154 and/or exhibited non-uniform stretching prior to breakage, with one segment appearing taut and
155 adjacent segments appearing slack, followed by breakage of the bridge within the taut segment (23
156 of 25 cases examined, Fig. 1D, Movie S7). Supporting the idea that local actomyosin contractile
157 forces contribute to bridge breakage, live cell imaging with the actin reporter RFP-Utr261 (*32*)
158 revealed large concentrations of actin filaments immediately adjacent to the taut segments of the

bioRxiv preprint doi: https://doi.org/10.1101/835058; this version posted November 7, 2019. The copyright holder for this preprint (which was not peer-reviewed) is the author/funder, who has granted bioRxiv a license to display the preprint in perpetuity. All rights reserved. No reuse allowed without permission.

bridge just prior to breakage in all cases examined (n = 30; Fig. 1E, Fig. S5A, Movies S8-9 and see (*27*) for similar results). Actin accumulation was transient and dissolved after bridge breakage. Immunostaining to detect paxillin revealed large focal adhesions at sites of F-actin accumulation where bridges appeared taut, indicating strong cell-extracellular matrix attachments (Fig. 1F). These sites also had extensive accumulations of non-muscle myosin II, which co-stained for the active, phosphorylated form of myosin regulatory light chain, indicating high contractile forces (Fig. 1G). Local myosin accumulation and contractility is known to be induced by increased membrane tension (*33*), which is expected to occur at the base of extending chromosome bridges.

We next asked if actomyosin contractility is required for chromosome bridge breakage. During live imaging, chromosome bridges were generated and allowed to extend, and then small-molecule inhibitors of myosin activation (ML7) or actin assembly (Latrunculin A) were added. By comparison with controls, ML7 addition substantially delayed, and Latrunculin A addition abolished, bridge breakage (Fig. 1H, Fig. S5B, and Movie S10) demonstrating that a functional actomyosin network is required for bridge breakage. Moreover, when cells were plated on fibronectin, which increases focal adhesions and intracellular actomyosin contractile forces (*34*), bridge breakage was accelerated two-fold ($p < 0.0001$; Fig 1I). Because fibronectin also affects cell signaling (*35, 36*), we plated cells on hydrogels of varying stiffness, all coated with the same concentration of fibronectin. Consistent with the known effect of reduced substrate stiffness diminishing actomyosin contractility (*37*), bridge lifetime increased with decreasing substrate stiffness (Fig. 1J). Finally, we asked whether bridge breakage depends on the LINC complex, the best characterized pathway by which actomyosin forces can be transmitted across the nuclear envelope (*38-40*). Knockout of the major inner nuclear membrane LINC components, SUN1 and SUN2, had a partial effect, delaying bridge breakage ($t_{1/2}$ = 18 hr; Fig 1K and Fig. S6). Together,

182 these data establish a critical role for cytoplasmic actomyosin contractile forces in chromosome
183 bridge breakage.
184
185 **Single-cell sequencing reveals the immediate impact of chromosome bridge breakage**
186 *Copy number alterations immediately after bridge breakage*. We investigated both the
187 immediate and long-term consequences of chromosome bridge breakage on genome structure. To
188 define the immediate outcome(s) of bridge breakage, we employed our previously developed
189 approach, which combines live-cell imaging with single-cell whole-genome sequencing [Look-
190 Seq (*17*)]. Chromosome bridges were induced, their breakage was monitored by live-cell imaging,
191 and the two daughter cells were isolated ~8 hr after bridge breakage for single-cell whole genome
192 sequencing. Sequencing was performed to ~25× mean depth, which allowed us to interrogate
193 ~90% of the unique sequence of each homologous chromosome with one or more reads (Fig. 2A,
194 Methods). This approach enabled us to observe the immediate consequences of bridge breakage
195 without confounding genomic alterations during subsequent cell divisions.
196 In all 20 cell pairs after bridge breakage, we observed copy number alterations affecting a
197 segment (>2.5 Mb) of one or more chromosome arms, distributed in a reciprocal pattern between
198 the daughter cells (Fig. 2B, Fig. S7, and Movies S11-13). Using previously developed haplotype
199 copy number analysis, we could unambiguously identify the homologous chromosome that
200 underwent breakage (*17*) . Most commonly, we found terminal segment reciprocal gain and loss
201 patterns, which, as in the original BFB model (*21*), are expected from breakage of dicentric fusions
202 between sister chromatids or single chromatids from different chromosomes ("chromatid fusions,"
203 Fig. 2C). Interestingly, in four daughter cell pairs, we observed the reciprocal gain and loss of
204 internal chromosome segments. This pattern can be explained by breakage of replicated dicentric

bioRxiv preprint doi: https://doi.org/10.1101/835058; this version posted November 7, 2019. The copyright holder for this preprint (which was not peer-reviewed) is the author/funder, who has granted bioRxiv a license to display the preprint in perpetuity. All rights reserved. No reuse allowed without permission.

chromosomes derived from two different chromosomes ("chromosome fusions," (*41*), Fig. 2D), coupled to an inverted orientation of the dicentric chromatids along the mitotic spindle. Although bridge breakage sometimes affected only one chromosome, in nine cases, two or more different chromosomes were involved, as expected from the methods employed to induce bridges (*41*); the exception was the CRISPR-based method, which, as expected, exclusively produced chromosome 4 bridges (Fig. 2B).

Closer inspection of the bridge breakpoints revealed a spectrum of genomic outcomes, where some bridges underwent simple breakage and others experienced fragmentation, which was specifically localized to the region of the main copy number transition (Fig. 3). In cases where bridge breakage occurred with local fragmentation, fragments as small as ~100 kb could be readily detected (see Methods for details) if these fragments were retained within a larger region of complete haplotype loss. The retention of larger (~1Mb) fragments in one daughter could also be validated by reciprocal loss of this fragment in the sister cell. Rearrangements involving fragment ends often provided additional support for the identification of fragmentation.

Importantly, both simple breaks and local fragmentation could be generated by mechanical force-dependent bridge breakage, because direct breakage of bridges with a glass capillary yielded a very similar spectrum of outcomes (Fig. 4A and Fig. S8A). Moreover, we observed similar local fragmentation patterns for spontaneous bridge breakage in TREX1-null cells, reinforcing the conclusion that TREX1 is not required to break or fragment chromosome bridges (Fig. 4B and Fig. S8B).

In sum, these findings demonstrate that the immediate consequences of bridge breakage are relatively simple patterns of copy number alterations localized to the bridge. This localized pattern contrasts with that reported from bulk sequencing of populations of cells isolated many

generations after telomere crisis. These populations often contained complex copy number oscillations and rearrangements that encompassed most of a chromosome arm and/or spanned the centromere (*26*). We also observed these complex patterns in long-term population evolution experiments and will present evidence defining a cascade of events downstream of initial bridge breakage that can explain them (see Figs. 7-9 below).

Chromosome rearrangements associated with bridge breakage. We next analyzed chromosome rearrangements associated with the above described DNA copy number alterations. Many cell pairs exhibiting simple breakage or small-scale fragmentation contained the approximate number of rearrangements expected from ligation of the fragments (Fig. 3B). This pattern of rearrangements closely resembles what has been termed "local jump footprints," a rearrangement signature in cancer genomes of unknown origin (*42*). We also identified several examples of local fragmentation involving two or more chromosomes, where subsequent end-joining produced a pattern of intra- and inter-chromosomal rearrangements (Fig. 3C, bottom cell). Overall, these findings suggest that "local jumps" can be generated by DNA ligation after local fragmentation, and thus may share a common underlying mechanism with many cases of chromothripsis, consistent with our previous proposal (*17*).

Four daughter cell pairs showed a distinct and particularly extreme pattern of complex rearrangement (n = 4 of 20 cell pairs; Fig. 5A). In two of these cases we additionally observed kataegis near the rearrangements. Kataegis is a phenomenon in which local clusters of point mutations are generated in a strand-coordinated manner and in trinucleotide contexts implicating the action of APOBEC family cytosine deaminases on single-stranded DNA (Fig. S9) (*43, 44*). Thus, complex rearrangements and kataegis can occur at or around the time of chromosome bridge breakage, albeit in a minority of cases.

Analysis of rearrangement junctions from these four samples revealed surprising features that are inconsistent with an origin from simple fragmentation followed by ligation in random order and orientation. Instead, the rearrangement pattern suggests it originates from errors during DNA replication. First, rather than being randomly distributed, in these samples, breakpoints were tightly clustered into local hotspots, as has been previously noted in chromothripsis samples but not understood mechanistically (*45*). Second, tracking the connections between rearrangements revealed chains of short insertions (median 183 bp) that were arrayed in tandem, hereafter referred to as "Tandem Short Template" (TST) jumps (Fig. 5B). The TST insertions were typically derived from multiple hotspots on chromosomes within the bridge, but occasionally, insertions originated from other chromosomes not involved in the bridge. One plausible explanation is that these insertions were generated by template-switching DNA replication errors, as in the microhomology-mediated break-induced replication (MMBIR) model (*12, 46*).

Accordingly, we analyzed microhomology at the junctions between TST insertions. Although a minority of junctions showed blunt-end joining (≤ 1bp microhomology), junctions with microhomology were also infrequent. For example, of the 13 junctions in the TST chain shown in Fig. 5B, five contained microhomology or insertion of ≤1 bp, and two showed ≥2 bp microhomology. The remaining six junctions contained 2–20 bp of sequence with ambiguous origin. It is possible that these sequences reflect junctional microhomology, but that detection of microhomology is obscured because the sequences are derived from repeats and/or partial mismatches that are difficult to map (*47*).

In light of the above findings implicating aberrant DNA replication in the generation of the TST jump signature, we characterized the efficiency of DNA replication in chromosome bridges. Pulse-labeling with the nucleoside analog, 5-ethynyl-2′-deoxyuridine (EdU) was used to assess

bioRxiv preprint doi: https://doi.org/10.1101/835058. this version posted November 7, 2019. The copyright holder for this preprint (which was not peer-reviewed) is the author/funder, who has granted bioRxiv a license to display the preprint in perpetuity. All rights reserved. No reuse allowed without permission.

replication in chromosome bridges. Cells in S phase labeled strongly for EdU in the primary nucleus, but EdU intensity dropped off where chromatin extruded from the main nucleus and was absent from most of the bridge (Fig. 5C). Control experiments demonstrated that the absence of EdU signal was not due to limited detection sensitivity for the small amount of DNA in bridges (Fig. S10). The same defect was observed in intact bridges and broken bridge stubs (Fig. 5C), indicating that both structures have replication defects. Further support for the conclusion that bridge DNA is poorly replicated came from our single-cell sequencing experiments. In approximately half of the daughter cell pairs, we could identify a region of the bridge chromosome that was present at lower copy number than the intact homologue that was not in the bridge (Fig. 5D). Therefore, chromosome bridges exhibit severe DNA replication defects similar to those previously identified in micronuclei (*14, 16, 19*).

We observed the TST jump signature in two additional contexts by bulk DNA sequencing. First, we identified the TST jump signature by bulk sequencing of a population of cells derived from a single cell with a broken bridge. We use CRISPR to induce breakage of the termini of Chr4, observed the formation and breakage of chromosome bridges and then isolated individual cells that were then grown into large populations (>10^6 cells each). One out of 12 such populations evidenced clustering of rearrangements into breakpoint hotspots, with chains of short insertions with a similar size range as the single cell experiments (Fig. 6A). Second, we identified the TST jump signature by long-read sequencing of a primary tumor sample obtained from a patient with renal cell carcinoma. In this patient sample, the TST jumps are associated with a chromothripsis event that generated the unbalanced translocation between Chr3p and Chr5q (Fig. 6B), which is the canonical driver event in this cancer type (*48*). The median size of the insertions (199 bp) was similar to what we observed by single-cell sequencing of broken bridges (Fig. 6C). These findings

297 indicate that the TST jump signature reflects a specific mutational process that can be stably
298 inherited over many generations.

299 In summary, sequencing cells after the breakage of chromosome bridges demonstrates that
300 most rearrangements result from ligation after localized fragmentation but that highly complex
301 rearrangements do occur in a minority of cases. The unique sequence features of these
302 rearrangements (TST jumps) suggest an origin from template-switching errors in DNA replication
303 (*12, 47, 49, 50*).

304

305 **Mechanisms generating DNA damage downstream of chromosome bridge breakage**

306 *Damage from aberrant mitotic DNA replication*. Although there is a low frequency of
307 complex rearrangement initially associated with chromosome bridges in the first interphase after
308 the bridge has formed, we hypothesized that additional DNA damage might arise downstream of
309 bridge breakage. First, chromosome bridges contain segments of incomplete DNA replication and
310 probably stalled replication forks that could undergo replication fork breakage upon entry into
311 mitosis (*51, 52*). Second, we found that complex rearrangements were frequent in the second
312 generation (i.e. grand-daughter cells) derived from cells with the stubs of broken chromosome
313 bridges. In all three of the second-generation lineages that we examined by single-cell sequencing,
314 we detected complex rearrangements localized near the bridge breakpoints (Fig. S11). These
315 considerations motivated experiments to determine if the broken stubs of chromosome bridges
316 acquire additional damage upon entry into the next mitosis.

317 We assayed DNA damage in mitosis using a protocol of live-cell imaging followed by
318 fixation and staining for γ-H2AX in these same cells. Relative to primary nuclei, most broken
319 bridges exhibited little to no detectable damage during interphase, even when cells were held in

bioRxiv preprint doi: https://doi.org/10.1101/835058. this version posted November 7, 2019. The copyright holder for this preprint (which was not peer-reviewed) is the author/funder, who has granted bioRxiv a license to display the preprint in perpetuity. All rights reserved. No reuse allowed without permission.

extended G2-arrest with CDK1 inhibition. However, if cells with broken bridge stubs were released into mitosis, γ-H2AX labeling intensity increased ~5-fold (Fig 7A-B). This damage was localized to one or a few mitotic chromosomes and was observed only in cells that had a bridge in the prior interphase (Fig 7A). Heavy mitotic γ-H2AX labeling was consistently associated with extensive replication protein A (RPA) accumulation, indicating the generation of single-stranded DNA (ssDNA) (Fig. 7A-B). Surprisingly, pulse-labeling with EdU revealed that RPA and γ-H2AX accumulation coincided with extensive DNA synthesis that occurred specifically on the bridge DNA during mitosis (Fig. 7C). Similar findings were obtained in BJ cells with bridges induced by topoisomerase inhibition (Fig. S12). Live-cell imaging of GFP-RPA2 established that the mitotic replication specifically occurred on the stub of the broken chromosome bridge (Fig. 7D and Movie S14). Therefore, the stubs of broken chromosome bridges undergo a second wave of DNA damage during a burst of aberrant, mitosis-specific DNA replication.

Chromosome bridges generate micronuclei. If chromosome bridge formation generated micronuclei, the frequency of chromothripsis and the size of the rearrangement footprint would be further increased (*14, 17*). This could contribute to the extensive pattern of rearrangements previously reported by bulk sequencing of cell clones derived after telomere crisis (*26*).

Although it has been previously reported that there is no increase in the frequency of micronuclei immediately after chromosome bridge breakage (*26*), whether the resulting broken chromosomes segregate normally in subsequent cell divisions has not been examined. To address this question, we used live-cell imaging to track these chromosomes over two generations (Fig. 8A). We confirmed that micronucleation is not an immediate consequence of chromosome bridge breakage in the first cell cycle when the bridge forms and breaks. However, a different result was obtained when we examined daughter cells with broken bridges that went through the next mitosis:

bioRxiv preprint doi: https://doi.org/10.1101/835058. this version posted November 7, 2019. The copyright holder for this preprint (which was not peer-reviewed) is the author/funder. All rights reserved. No reuse allowed without permission.

343 52% of divisions resulted in grand-daughter cells with micronuclei (n = 82 daughter cell divisions
344 examined; Fig. 8A and Fig. S13A). This frequency was higher still when the bridge did not break
345 during the first cell division (65%, n = 20). By comparison, cells without a bridge divided normally
346 and did not produce micronuclei (n = 82 divisions), even though they were present in the same
347 imaging dish and were treated identically. BJ cells induced to form bridges by topoisomerase
348 inhibition also showed an increase in micronucleation rate (>5 fold) in the second cell cycle (Fig.
349 S13A). Therefore, micronucleation is a major downstream consequence of chromosome bridge
350 formation.

351 To determine whether the above described micronuclei contain chromosomes from
352 bridges, we generated CRISPR-mediated Chr4 bridges and used fluorescence in situ hybridization
353 (FISH) to detect DNA from Chr4 (Fig. 8B). In the first cell cycle after induction, almost all bridges
354 contained Chr4 sequence (Fig. S1C). Chr4 centromeres (CEN4) sometimes localized to the "base"
355 of the bridge, with some CEN4 spots appearing stretched, suggesting that they were under
356 mechanical tension (Fig. 8B). In the second cell cycle, most micronuclei contained DNA from
357 Chr4 (80%, n = 105), indicating that the majority of chromosomes from bridges mis-segregate in
358 the next mitosis. Surprisingly, most of these micronuclei contained CEN4 DNA (62%, n = 84),
359 indicating that the high rate of mis-segregation cannot be explained by loss of centromeric DNA.
360 As most bridge-derived micronuclei exhibited little or no staining for CENP-A (Fig. S13B), it
361 appeared that the functionality of centromeres trapped within bridges might be compromised.

362 Defective loading of CENP-A, presumably due to nuclear import defects, could contribute
363 to centromere defects in chromosome bridges, as was recently reported for micronuclei (*53*).
364 However, failure to load new CENP-A would only cause a 2-fold dilution each cell cycle, which
365 on its own (*54*) would be unlikely to explain the timing and extent of chromosome mis-segregation

bioRxiv preprint doi: https://doi.org/10.1101/835058. this version posted November 7, 2019. The copyright holder for this preprint (which was not peer-reviewed) is the author/funder, who has granted bioRxiv a license to display the preprint in perpetuity. All rights reserved. No reuse allowed without permission.

366 we observed. This frequent mis-segregation suggested a more severe defect, perhaps due to active
367 stripping of previously loaded CENP-A from the centromeres of bridge chromosomes. To address
368 this possibility, we pulse-labeled cells expressing Halo-tagged CENP-A from its endogenous locus
369 (*55*) prior to the induction of chromosome bridges, enabling preferential visualization of the
370 preexisting population of CENP-A that was loaded prior to bridge formation. After labeling and
371 bridge induction (TRF2-DN), cells were given sufficient time to divide twice—first to form
372 bridges, and again to allow bridges to be converted to micronuclei (Fig. 8C). We then measured
373 CENP-A levels at centromeres in micronuclei and determined that they were reduced ~4-fold
374 relative to the primary nucleus, with ~25% of micronuclear centromeres lacking any detectable
375 CENP-A (Fig. 8C). By contrast, in control micronuclei induced by nocodazole washout, CENP-A
376 levels were only ~1.5-fold reduced using the same labeling strategy (Fig. S13C), as expected from
377 defective CENP-A loading alone. Therefore, chromosomes in bridges are prone to CENP-A
378 depletion, which likely compromises centromere identity, leading to frequent micronucleation and
379 additional chromothripsis.
380
381 **Common mechanisms for DNA damage in micronuclei and chromosome bridges**
382 We hypothesized that chromosome bridges and micronuclei, although morphologically
383 distinct, might nevertheless have a similarly defective nucleoplasm leading to similar defects in
384 DNA replication—both during interphase and then later in mitosis. This idea was motivated by
385 our previous work showing that the replication defect in micronuclei stems from aberrant nuclear
386 envelope assembly and defective nucleo-cytoplasmic transport (*19*). Chromosome bridges share
387 this same defect in nuclear envelope assembly (*19*).

388 We determined if micronuclei acquire DNA damage during interphase like chromosome
389 bridges. Because nuclear envelope disruption itself causes DNA damage (*18*), we characterized
390 micronuclei with intact nuclear envelopes. Micronuclei were generated by a nocodazole washout
391 procedure (*17*) and EdU labeling was used to assess the extent of DNA replication in micronuclei
392 relative to the primary nucleus (Fig. 9A). Intact micronuclei were identified by their accumulation
393 of a nuclear import reporter (RFP fused with a nuclear localization signal, RFP-NLS) (*17*). As
394 expected, many micronuclei in G2 cells had detectable, but strongly reduced DNA replication
395 relative to the primary nucleus (median EdU ratio = 27%). In these G2 cells, 23% of intact
396 micronuclei displayed DNA damage (Fig. 9A-B). Interestingly, almost all DNA damage occurred
397 in micronuclei with the strongest replication defect, as 90% of damaged micronuclei were at or
398 below the median EdU level (27% of the primary nucleus signal, Fig. 9A-B). Furthermore, nearly
399 all DNA damage in intact micronuclei could be eliminated by blocking the initiation of DNA
400 replication with small molecule inhibitors of either cyclin-dependent kinase (CDK) or Dbf4-
401 dependent kinase (DDK) (Fig. 9A-B). We note that although γ-H2AX intensity measurements
402 were reliable for assessing DNA damage in micronuclei, similar measurements are not feasible for
403 chromosome bridges because of the tension-induced nucleosome loss that occurs on bridge
404 chromosomes (*26*). Single-cell sequencing showed extensive chromothripsis-like rearrangements
405 in one of ten G2 cells with intact micronuclei (Fig. 9C). Thus, like chromosome bridges, intact
406 micronuclei undergo defective DNA replication in interphase during the first cell cycle after their
407 formation, leading to a low frequency of DNA damage and chromothripsis.

408 We next asked if micronuclear chromosomes, like broken chromosome bridges, undergo
409 mitotic replication and secondary DNA damage. Although most intact micronuclei in G2 cells
410 lacked DNA damage, after entering mitosis, there was a ~10-fold increase in damage levels on

bioRxiv preprint doi: https://doi.org/10.1101/835058. this version posted November 7, 2019. The copyright holder for this preprint (which was not peer-reviewed) is the author/funder, who has granted bioRxiv a license to display the preprint in perpetuity. All rights reserved. No reuse allowed without permission.

411 micronuclear chromosomes, accompanied by mitotic DNA synthesis and the accumulation of
412 ssDNA (Fig. 9D-F, Fig. S14A, and Movie S15). These findings were corroborated in BJ and HeLa
413 cells (Fig. S14B).

414 We used single-cell sequencing to determine if transit through mitosis promotes complex
415 rearrangement of micronuclear chromosomes. By live-cell imaging, we identified cells with intact
416 micronuclei that subsequently went through mitosis, generating daughter cells. Unlike the parental
417 G2 cells where only one of ten cells exhibited chromothripsis (Fig. 9C), we observed
418 chromothripsis in eight of the nine daughter pairs after passing through mitosis (Fig. 9G and Fig.
419 S15). Thus, incompletely replicated chromosomes from either micronuclei or bridges undergo
420 aberrant replication upon entry into mitosis linked to a high frequency of complex rearrangement
421 in the next generation.

422 Therefore, at a low frequency, DNA from chromosome bridges or micronuclei undergo
423 fragmentation and rearrangement during defective DNA replication in interphase. Subsequently,
424 a second wave of abnormal replication and heavy DNA damage occurs when cells enter mitosis.
425 For chromosomes bridges, DNA damage and chromothripsis is further amplified by the induction
426 of micronuclei.

427

428 **Complex genome evolution from the formation of a chromosome bridge**

429 Our results identify a cascade of events that should amplify both the frequency and extent
430 of chromosomal aberrations downstream of chromosome bridge formation. These findings predict
431 that the formation of a chromosome bridge should initiate ongoing genome instability where
432 episodes of chromothripsis would necessarily accompany breakage-fusion-bridge cycles (*3, 56*).

bioRxiv preprint doi: https://doi.org/10.1101/835058. this version posted November 7, 2019. The copyright holder for this preprint (which was not peer-reviewed) is the author/funder, who has granted bioRxiv a license to display the preprint in perpetuity. All rights reserved. No reuse allowed without permission.

To more directly test our model, we induced the formation of CRISPR-generated Chr4 bridges as discussed above, enabling us to track the evolution of the bridge chromosome in a long-term population growth assay. Bulk genome sequencing analysis of 12 such populations (hereafter "primary clones") revealed copy number alterations that affected one or both copies of Chr4 in every primary clone (Fig. 10A, Fig. S16). Only one primary clone showed simple breakage of Chr4, whereas the remainder showed complex copy number patterns and rearrangements: seven primary clones had complex copy number alterations confined to one arm of Chr4, and four exhibited alterations of both Chr4 arms (Fig. S16).

Across all 12 primary clones, there were 26 additional karyotype abnormalities (copy number alterations and/or chromosome fusions) affecting a total of 8 different non-targeted chromosomes (Table S1). Interestingly, these fusions primarily involved acrocentric chromosomes (85% of cases), which were typically seen fused at their p-arms to the aberrant Chr4 (Fig. S17). A similar enrichment of acrocentric fusions has been reported previously in samples after TRF2-DN expression (*57*), so this effect is unlikely to be an off-target artifact of the CRISPR-generated Chr4 bridge system. These results suggest that broken chromosome ends might be more likely to fuse with acrocentric chromosomes whose terminal rDNA repeat sequences are fragile and prone to spontaneous breakage (*58*). The high frequency of acrocentric fusions may also be explained by selection, as they provide an efficient path to stabilize broken bridge chromosomes by supplying a single functional centromere and telomere. Importantly, the non-Chr4 aberrations were typically subclonal within each primary clone (Table S1), suggesting their occurrence during downstream evolution of the initial bridge involving Chr4.

Multiple additional lines of evidence indicated a high degree of ongoing genome instability within most of the primary clones, including (i) high frequencies of micronuclei and chromosome

456 bridges (not shown); (ii) non-clonal aberrations of Chr4 observed by cytogenetic analyses (Table
457 S1 and Fig. S17); and (iii) non-integer copy number states in the bulk sequencing data, indicating
458 subclonal copy number heterogeneity (Fig. 10A, Fig. S16, and Fig. S18). Subclonal heterogeneity
459 was directly validated with low-pass sequencing followed by DNA copy number analysis on
460 ~500–800 single cells from each of nine primary clones (Fig. 10B and Fig. S19). This
461 heterogeneity primarily occurred on Chr4, but was also evident on acrocentric Chrs 13, 14, 15, and
462 22 at lower penetrance (Fig. 10B and Fig. S19).

463 To better understand the evolution of copy number variation, we derived subclones from
464 the primary clones, and performed bulk whole-genome sequencing (Fig. 10C-D). These data
465 provided clear evidence for complex copy number alterations and rearrangements occurring
466 downstream of the initial bridge breakage event. Three representative subclone copy number
467 profiles, shown in Fig. 10C, illustrate a shared ancestral breakpoint near the Chr4 p-arm terminus
468 (dotted black line), as well as additional breakpoints specific to each lineage (dotted blue lines).
469 The breakpoints private to each lineage cannot be explained by an early rearrangement event with
470 subsequent loss in some subclones. Instead, these breakpoints can only have been acquired after
471 the ancestral break.

472 Other examples provided evidence for least three modes of ongoing genome evolution in
473 the primary clone. First, we observed kataegis in 22 of 23 subclones derived from primary clone
474 1a; however, only a few of these kataegis events were shared across the entire set of subclones
475 (Fig. S20). Most kataegis events were identified only in particular lineages or were even private to
476 just one subclone, which is best explained by some kataegis events occurring late in the evolution
477 of the population (Fig. S20). Second, as shown by the analysis of subclones from one primary
478 clone in Fig. 10D, one homolog (homolog A) exhibited shared breaks as well as private focal

479 changes, including amplifications, which varied in both magnitude and location across the
480 different subclones. Third, in other subclones from this experiment that all share a common
481 homolog A profile, we observed variable loss of the p-arm terminus for homolog B in a pattern
482 suggestive of progressive shortening. This finding, together with our observation that one
483 subclonal lineage exhibits an intact homolog B profile (Fig. 10D bottom), indicates that the
484 evolution of homolog B occurred late during growth of the primary clone and postdated the
485 alterations that gave rise to their shared homolog A profile.

486 The apparent progressive shortening of homolog B in Fig. 10D likely reflects ongoing BFB
487 cycles. The absence of cells with gain of this region, as predicted by the BFB model, may be
488 explained by gene amplification compromising the fitness of these cells, and/or a bias towards
489 segmental loss due to under-replication of bridge DNA (Fig. 5C-D). This progressive pattern of
490 terminal segment loss generates a sloping average copy number level in the bulk sequencing data
491 (Fig. 10D, homolog B). This pattern is present in most of our primary clones (Fig. S18), and is
492 also commonly observed in cancer genomes (C.Z. Zhang, unpublished). The pattern may therefore
493 represent a useful sequence-based biomarker for ongoing genome instability.

494 In summary, our results demonstrate that the formation and breakage of a chromosome
495 bridge initiates a cascade of events that rapidly generate a high degree of genomic complexity and
496 cellular heterogeneity. Because later genome evolution obscures the initial genomic alterations,
497 elucidating early events requires a combination of live-cell imaging and single cell genomic
498 analysis (Look-Seq), enabling a direct correspondence to be established between the phenotype of
499 a cell division error and its genomic consequences.
500

DISCUSSION

Our results identify a cascade of events that generate increasing amounts of chromothripsis after the formation of a chromosome bridge. These findings substantially revise the chromosome breakage-fusion-bridge model (*21, 59, 60*) and establish that episodes of chromothripsis will be inherently interwoven with BFB cycles, explaining the implied association between these processes in cancer genomes.

We propose the following model (Fig. S21). Like micronuclei, nuclear envelope assembly around chromosome bridges is aberrant, leading to a depletion of nuclear pores (*19*) and a defective nucleoplasm. This results in poor DNA replication in the bridge, including stalled replication forks and replication origins that have not fired. The bridge is then broken by a mechanism that requires stretching force from the actin cytoskeleton. Bridge breakage produces simple breaks and local fragmentation, generating free DNA ends that can engage in end-joining and/or in error-prone replicative repair, potentially MMBIR (*12, 46*). In some cells, this produces the rearrangement signature that we term Tandem Short Template (TST) jumps. These events lead to a low frequency of chromothripsis during the interphase when the bridge forms and breaks. Subsequently, after cells enter mitosis, the stubs of broken chromosome bridges undergo a burst of aberrant mitotic DNA replication, similar to what occurs for micronuclear chromosmes. This leads to significantly more DNA damage and increases the frequency of chromothripsis. Finally, bridge formation disrupts the centromere histone epigenetic mark, compromises centromere function and thereby increases the rate of micronucleation during the next cell division after bridge formation. These micronuclei generate further cycles of chromothripsis, as previously described (*15, 17*). Combined, these mutational events rapidly generate hallmark features of cancer genome complexity,

523 producing continuing cycles of genome evolution and subclonal heterogeneity from a single cell
524 division error.

525

526 **Mutagenesis and DNA fragmentation from actomyosin-based force**

527 It was previously proposed that bridge breakage might occur by mechanical forces
528 generated during chromosome segregation in mitosis (*21*), cytokinetic furrow ingression, or
529 abscission (*24, 25*). However, recent findings (*26*) and our own observations indicate that most
530 bridges remain intact throughout mitosis, cytokinesis, and abscission, arguing against a major role
531 for these processes in bridge breakage. This work suggested that bridges are cleaved enzymatically
532 via a mechanism partially dependent upon the cytoplasmic, endomembrane-associated
533 exonuclease TREX1 (*26*). Our data disfavor a role for TREX1 and, instead, demonstrate that
534 bridge breakage requires mechanical forces from interphase actomyosin-based contractility (Fig.
535 1). These forces appear to be exerted locally on DNA near the base of the bridge and are associated
536 with transient actin accumulation and large focal adhesions. This actin accumulation may be
537 triggered by plasma membrane tension, consistent with well-described force-response properties
538 of cytoskeletal contractility (*37, 61, 62*). Actomyosin forces are transmitted across the nuclear
539 envelope to the bridge chromatin in part by the LINC complex (*38, 40*).

540 A simple interpretation of our results is that actomyosin-dependent forces are capable of
541 rupturing the phosphodiester bonds in bridge DNA. The force required to break DNA is estimated
542 to be in the range of 0.5–2 nN (*63, 64*), which can be achieved or exceeded by traction forces
543 generated from individual focal adhesions, which range from 2~20 nN (*37, 65-67*). Although non-
544 covalent interactions connecting actin to chromatin (LINC-dependent and -independent) are

545 individually weak, large numbers of attachments acting in parallel could support the high
546 mechanical load needed to break DNA.

547 It is also possible that bridge breakage involves DNA processing enzyme(s) whose activity
548 or access to DNA requires mechanical tension. Force-mediated ejection of nucleosomes from
549 DNA (*68*), which explains the rapid loss of histone signal we and others have observed in bridges
550 (*26*), might increase nuclease accessibility to bridge DNA. In principle, loss of nuclear envelope
551 integrity could enable access of cytoplasmic nucleases such as TREX1 (*26*); yet we observed that
552 knockout of TREX1 had no effect on bridge lifetime. Moreover, we did not detect an impact of
553 nuclear envelope rupture on bridge breakage, which disfavors a mechanism based on NE-restricted
554 access of cytoplasmic nucleases to bridge DNA. We therefore propose that mechanical force is
555 either sufficient for DNA breakage or facilitates the action of one or more nuclear-localized
556 factors, such as a nuclease or topoisomerase.

557 Whole-genome sequencing of single cells after chromosome bridge breakage during the
558 interphase after they were formed revealed that bridge breakage resulted in either simple breaks or
559 local DNA fragmentation, consistent with a breakage mechanism involving mechanical force.
560 Indeed, we also observed both simple breakage and fragmentation when we mechanically broke
561 intact chromosome bridges with a glass capillary. Mechanical bridge breakage could, in principle,
562 cause localized chromosome fragmentation if forces were applied to multiple sites on chromatin,
563 as might occur if the chromatin were in a looped conformation.

564 We highlight that our ability to draw mechanistic conclusions about bridge breakage
565 benefitted from specific features of our analysis and experimental design: haplotype-specific DNA
566 copy number measurement and the comparison of sister cells (Fig. 2). For example, we noted
567 puzzling examples of internal chromosome segment copy number alterations after bridge breakage

568 (Fig. 2C). Duplication of an internal chromosome segment, as we observed in those daughter cells
569 with copy number gain, would commonly be attributed to a DNA replication error involving
570 template switching or to unequal sister chromatid exchange between repeat sequences (*69*).
571 However, the comparison between sister cells instead showed this class of copy number alteration
572 in our experiments is best explained by DNA breakage after chromosome-type fusions.
573
574 **Chromosomal rearrangements from abnormal nuclear architecture**
575 When bridge breakage was accompanied by fragmentation, we often detected chromosome
576 rearrangements. In most cases, rearrangements resulted from ligation of fragments generated
577 during bridge breakage. This gave rise to a range of outcomes (Fig. 3), from simpler patterns
578 similar to the "local jump" footprint described in cancer genomes (*42*), to more complex events
579 meeting the criteria for chromothripsis (*45*). In cases where multiple chromosomes appeared to
580 be present in the bridge, we often also detected interchromosomal rearrangements between
581 breakage sites.
582 A subset of bridge breakage events (4 of 20) showed a distinct pattern of extreme localized
583 rearrangements, where small (~2–3 kb) regions contained focal clusters of ~10 breakpoints each.
584 These "hotspots" were extensively inter-connected by rearrangements, despite being situated
585 megabases apart in the reference genome or, occasionally, on different chromosomes. This
586 generates a signature of multiple short (median ~150–200 bp) insertions present in tandem within
587 rearrangement junctions (TST jumps; Fig. 5). We think TST jumps are likely generated by
588 aberrant DNA replication involving replication template switching (*12*) for the following reasons.
589 First, local breakpoint clusters are not expected from a random fragmentation process but could be
590 generated by localized cycles of replication fork collapse, breakage, and aberrant replicative repair.

591 Second, the size distribution of inserted segments (Fig. 6C) is inconsistent with random
592 fragmentation and re-ligation. In agreement with generally similar functional defects in
593 micronuclei and chromosome bridges, we previously identified an example of multiple short
594 tandem insertions in single cell analysis of chromothripsis derived from a micronucleus (*17*).

595 The TST jump signature does not result from artifacts during single-cell whole-genome
596 amplification because a similar pattern was observed in bulk sequencing analysis of clonal
597 populations of cells after bridge breakage. Furthermore, we also observed a similar signature by
598 long-read sequencing of a renal cell carcinoma genome. Features of the TST jump signature have
599 been described in large cancer data sets (*1, 70*) and tandem arrays of short insertions have also
600 been noted in lung cancer genomes, where they may be common ((*71*) and J. Lee, personal
601 communication). Although the cause of the TST jump signature is unknown, an origin for the
602 insertions from Okazaki fragments might explain the size distribution of the insertions, which is
603 strikingly similar in all of the contexts in which the pattern has been observed.

604 We demonstrate that similar DNA replication abnormalities occur in bridges and in
605 micronuclei whose nuclear envelopes are intact. This finding demonstrates that nuclear envelope
606 rupture (*18*) is not absolutely necessary for complex rearrangements on micronuclear
607 chromosomes. Common functional defects of the nucleoplasm in chromosome bridges and
608 micronuclei make sense, given these structures share a common defect in nuclear envelope
609 assembly (*19*). Generally, DNA replication errors are thought to be major sources of structural
610 variation in cancer genomes. However, what triggers these replication errors in the first place
611 remains poorly understood. We propose that nuclear architecture defects, a hallmark feature of
612 human cancer termed nuclear atypia (*72*) are a major trigger for cancer-associated DNA replication
613 errors.

bioRxiv preprint doi: https://doi.org/10.1101/835058; this version posted November 7, 2019. The copyright holder for this preprint (which was not peer-reviewed) is the author/funder, who has granted bioRxiv a license to display the preprint in perpetuity. All rights reserved. No reuse allowed without permission.

614

615 **A wave of DNA damage from aberrant mitotic DNA replication**

616 Based on the high frequency of chromothripsis after cells pass through mitosis, we
617 performed a series of experiments that uncovered an unexpected burst of DNA replication that
618 occurs during mitosis, specifically on the stubs of broken chromosome bridges or on micronuclear
619 chromosomes. This mitotic DNA replication is highly aberrant as it produces heavy DNA damage
620 and ssDNA formation. Although some ssDNA forms on bridges in interphase (*26*), the amount of
621 ssDNA is far greater in mitosis (Fig. 7). Mitotic replication may therefore make a significant
622 contribution to the kataegis pattern that has been linked to chromosome bridge breakage (Figs. S9
623 and S19; also see (*26*)).

624 The mechanism triggering mitotic DNA replication on bridge stubs or micronuclear
625 chromosomes is not known. However, because bridge and micronuclear DNA is incompletely
626 replicated during interphase, these structures likely contain stalled DNA replication forks and
627 licensed replication origins that have not fired. Our prior experiments demonstrate that for
628 micronuclei, incomplete DNA replication occurs because of defective nucleocytoplasmic
629 transport, leading to a failure to accumulate key proteins required for DNA replication and repair
630 (*14, 19*). However, when cells enter mitosis, the nuclear envelope surrounding the primary nucleus,
631 micronucleus or chromosome bridge will be broken down near-simultaneously. When this occurs,
632 under-replicated bridge or micronuclear DNA will suddenly gain access to the pool of replication
633 factors that had been sequestered in the primary nucleus throughout interphase. Access to
634 replication factors, coupled with high mitotic cyclin-dependent kinase activity (*51, 73*), likely then
635 activates replication on this incompletely replicated DNA. The DNA damage resulting from
636 mitotic DNA replication may have a number of causes including the well-described activation of

637 structure-specific endonucleases in mitosis (*74*) and/or the recently discovered cleavage of stalled
638 DNA replication forks that occurs because of removal of the MCM2-7 replicative helicase from
639 mitotic chromosomes (*51, 75*).
640
641 **Loss of the centromeric epigenetic mark in chromosome bridges**
642 In addition to the above described mutational events, we found that chromosome bridge
643 formation predisposes to micronucleation, which could then initiate another round of
644 chromothripsis downstream of bridge breakage (*14, 17, 76*). We attribute the high rate at which
645 bridge chromosomes mis-segregate in the second mitosis to depletion of CENP-A nucleosomes,
646 which provide the epigenetic specification of centromere identity (*77, 78*). Two mechanisms likely
647 contribute to CENP-A loss. First, because bridges largely lack nuclear pore complexes (*19, 26*)
648 and have dimensions that will impede diffusion (*79*), they should fail in the normal replenishment
649 of CENP-A nucleosomes that occurs each cell division. However, in the timeframe of our
650 experiments, this dilution cannot account for the observed magnitude of CENP-A loss. Instead,
651 our data suggests active CENP-A loss, which we propose may originate from stripping of CENP-
652 A containing nucleosomes by actomyosin forces when centromeric chromatin is trapped within
653 the bridge (Movie S16). The forces required to strip nucleosomes from DNA (~20 pN) are ~50-
654 fold lower than those required to break covalent bonds in the backbone (*63, 64, 68*). Thus, in
655 addition to promoting mutagenesis, actomyosin contractility may disrupt epigenetic marks on
656 chromatin.
657

bioRxiv preprint doi: https://doi.org/10.1101/835058. this version posted November 7, 2019. The copyright holder for this preprint (which was not peer-reviewed) is the author/funder, who has granted bioRxiv a license to display the preprint in perpetuity. All rights reserved. No reuse allowed without permission.

Rapid genome evolution from a single cell division error

The above described cascade of events is predicted to generate ongoing cycles of complex genome evolution. We tested this hypothesis with a CRISPR-based system to track the fate of a defined chromosome (Chr4) bridge. In populations derived from a single cell after bridge breakage, we detected extensive genetic heterogeneity, with evidence that chromothripsis recurs downstream of initial bridge breakage.

Together, these findings identify mechanisms that explain the remarkable potential of a single unrepaired DNA break to compromise the integrity of the genome. In human cells, a single DNA break only weakly, if at all, activates the DNA damage response to block cell cycle progression (*80, 81*). This means that unrepaired breaks can be amplified into many additional breaks when the cell divides due to the generation of micronuclei or additional chromosome bridges. Because de novo telomere addition is inefficient (*82*), stable end-capping of chromosomes is primarily achieved through chromosome translocation or break-induced DNA replication (*83*). For a stable chromosome to result, the DNA segment with the capped ends must additionally contain only one functional centromere. The end result is that downstream of chromosome bridge formation, it is easy for the accumulating burden of DNA breakage to exceed the capacity to stabilize broken DNA ends. Complex genome evolution with subclonal heterogeneity is therefore a virtually inevitable consequence of chromosome bridge formation, a common cell division error during tumor development.

bioRxiv preprint doi: https://doi.org/10.1101/835058. this version posted November 7, 2019. The copyright holder for this preprint (which was not peer-reviewed) is the author/funder, who has granted bioRxiv a license to display the preprint in perpetuity. All rights reserved. No reuse allowed without permission.

FIGURE LEGENDS

Figure 1. Chromosome bridge breakage requires actomyosin contractility.

(A) Indistinguishable chromosome bridge lifetimes observed with different experimental methods for bridge induction. Survival plot shows bridge lifetimes (time interval from bridge formation after mitosis until bridge breakage or the next mitosis; visualized with GFP-BAF). Methods of bridge induction were: inducible dominant-negative TRF2 (black, n = 624 bridges analyzed), partial knockdown of condensin (siSMC2, green, n = 119), low-dose topoisomerase II inhibition (100 nM ICRF-193, magenta, n = 121), and inducible CRISPR/Cas9-targeted telomere loss on chromosome 4 (Chr4g1, blue, n = 132). No significant difference in mean lifetime is found among the four methods ($p = 0.14$, one-way ANOVA).

(B) Extension of chromosome bridges is required for their breakage. Representative time-lapse images (GFP-BAF) of cells with bridges on "long" (20×300 μm, left) or "short" (20×100 μm, right) fibronectin micropatterns. Note: due to the area occupied by the main cell body of each daughter, bridge length does not exceed ~50 μm on short patterns. Dashed lines: micropattern borders; teal arrowheads: broken bridge ends. Timestamp is relative to completion of the previous mitosis (0 hr).

(C) Quantification of data from (B). Orange and teal traces show data for cells on short (n = 45) and long (n = 54) micropatterns; $p < 0.0001$ (Mann-Whitney).

(D) A representative chromosome bridge breakage event. Prior to breakage, there is apparent non-uniform stretching of the bridge (GFP-BAF). Magenta arrowhead indicates a transition between "taut" and "slack" regions of the bridge. The taut region appears to progressively stretch, whereas the slack region progressively retracts; breakage occurs in

the taut region. Inset images: high contrast of the regions marked by dashed red boxes to visualize the taut region before and after breakage. Timestamp is relative to bridge breakage (min).

(E) Actin dynamics during chromosome bridge breakage. Actin is detected with RFP-Utr261; bridges with GFP-BAF. Contraction of the actin-rich structure (magenta arrowheads) occurs immediately preceding and up to the time of bridge breakage (-25 to 0 min). After bridge breakage, the actin structure rapidly disassembles (20 min). Timestamp is relative to bridge breakage (min).

(F) Representative images show large focal adhesions (α-Paxillin) and actin fibers (phalloidin) at the bent region of a chromosome bridge (GFP-BAF), indicated by cyan arrowheads.

(G) As in (B), representative accumulation of contractile myosin II (α-myosin heavy chain, MHC; α-phospho-myosin light chain 2, pMLC2) at the transition between taut and slack segments of a chromosome bridge.

(H) Actomyosin contractility is required for bridge breakage. Bridge lifetime plots show the effect of actin disruption (0.5 μM Latrunculin A; red trace, n = 66) or myosin II inhibition (20 μM ML7; orange trace, n = 113) relative to controls (DMSO; black trace, n = 184). Cells were allowed to divide, form and extend chromosome bridges and were then exchanged into drug medium (see Fig. S5B).

(I) Increasing cellular contractility decreases bridge lifetime. Bridge lifetimes for cells plated on untreated glass (black, n = 148) or fibronectin (FN)-coated glass (light blue, n = 150).

(J) Bridge breakage depends on substrate stiffness. Bridge lifetimes were measured for cells plated on substrates of varying stiffness, each coated with 5 μg/ml fibronectin: glass (>10^6

kPa; light blue, n = 123), stiff gel (32 kPa; medium blue, n = 147), and soft gel (0.5 kPa; dark blue, n = 130).

(K) Bridge breakage in part requires the LINC complex. Bridge lifetimes for wild-type (black, n = 90), SUN1 knockout (orange, n = 90), SUN2 knockout (green, n = 90), and SUN1/SUN2 double knockout (red, n = 90) RPE-1 cells.

Figure 2. Immediate effect of chromosome bridge breakage on DNA copy number.

(A) Cartoon illustrating the Look-Seq experiment. Bridge formation and breakage was monitored during live imaging. After bridge breakage, individual daughter cells were isolated for whole-genome sequencing.

(B) Schematic summary of large-scale (≥2.5 Mb) DNA copy number alterations after bridge breakage. Dashed boxes show the p- and q-arms of each chromosome. Chromosome arms that contain a subregion with copy number alterations are colored as follows: white, diploid; red, gain; blue, loss; gray, copy-neutral loss of heterozygosity. Right: bridge lifetime and bridge length at the time of breakage for each sample.

(C) Type 1 events are daughter cells with reciprocal gain and loss of a terminal chromosome segment. Cartoon depicts chromatid fusion events initiated by DNA breaks or telomere uncapping. Left: sister chromatid fusion; Right: fusion of single chromatids from different chromosomes (G2 cell). The resulting dicentric fusions are segregated in mitosis (green dashed arrows) to form a bridge. Breakage of the bridge (dashed red line) generates the depicted reciprocal copy number alterations. Bottom: representative plot of DNA copy number (gray dots show mean copy number of 1-Mb bins) for the affected haplotype resulting from a Type 1 bridge breakage event involving the q-arm of chromosome 2. Red bar: inferred bridge breakpoint. Light gray bar: centromere.

(D) Type 2 events are reciprocal gain and loss of an internal chromosome segment between the daughter cells. Top: cartoon depicts a chromosome fusion (*28*) (e.g. from replication of an interchromosomal fusion occurring in G1). If the kinetochores of the dicentric chromatids attach to microtubule bundles from opposite poles (dashed green arrows), one dicentric will assume an inverted orientation relative to the other (middle panel). In contrast to the scenarios depicted in (C), cleavage of both chromatids in the resulting bridge at the indicated position yields reciprocal copy number alterations of an internal chromosome segment. Bottom, plot of DNA copy number as in (C).

Figure 3. Small-scale, highly localized DNA breakage and rearrangement with bridge breakage.

(A) Simple breakage of a bridge chromosome. Left: CIRCOS plots showing the bridge chromosome (Chr4) in the 4-2 daughter pair (Fig. 3B). DNA copy number is shown for the bridge haplotype (gray bars/black outline) and the non-bridge haplotype (white bars/grey outline); intrachromosomal rearrangements are shown as green arcs, chromosome band pattern is shown in the outer arc. Red arrowhead indicates the bridge breakpoint. Right: Expanded view of DNA copy number at the breakpoint transition (gray dots show 250-kb bins). Copy-number segments (red solid lines) are determined using SNP-level coverage in the top daughter (see Methods). The reciprocal pattern is shown for the bottom daughter (red dashed lines). This line represents the expected copy number in the bottom daughter based on fragmentation detected in the top daughter, assuming that two copies of the shown homolog were distributed between both daughters. Structural variants (SV) are shown above the copy-number plots as in the CIRCOS plots.

(B) Generation of the "local jump" pattern from bridge breakage. As in (A), shown are CIRCOS plots (Left) and DNA copy number plots with rearrangements (Right) for the bridge chromosome (Chr4) in the 4-4 daughter pair.

(C) Local fragmentation with complex rearrangement associated with bridge breakage. As in (A), CIRCOS plots (Left) and DNA copy number plots with rearrangement (Right) in the C-2 daughter pair, whose bridge contained three different chromosomes (Chrs 4, 5, and 6). Each bridge chromosome contains multiple breaks resulting in local fragmentation. The pattern of rearrangements in daughter (b) indicates end-joining of these fragments, including the formation of inter-chromosomal rearrangements (orange arcs or lines). In addition to fragmentation, daughter (a) evidences the TST jump rearrangement pattern (see Fig. 5).

Figure 4. Local fragmentation accompanies mechanical breakage of bridges and does not require TREX1.

(A) Mechanical breakage of chromosome bridges produces a spectrum of outcomes from simple breakage to local fragmentation. Left: schematic of the experiment using a glass capillary to mechanically stretch and break chromosome bridges. The daughter cells were collected for sequencing immediately after mechanical bridge breakage, to determine its direct consequences. Therefore, cells did not have time for DNA repair to generate chromosomal rearrangements. Top right: an example of simple bridge breakage. Plots as in Fig. 3, with the exception that grey dots in the whole-chromosome plot indicate 1 Mb bins due to lower (5×) sequence depth. Bottom right: two examples of local fragmentation.

(B) A similar spectrum from simple breakage to local fragmentation after spontaneous bridge breakage in cells lacking TREX1. Left: DNA copy number plots, as in (A), showing simple

bioRxiv preprint doi: https://doi.org/10.1101/835058. this version posted November 7, 2019. The copyright holder for this preprint (which was not peer-reviewed) is the author/funder. All rights reserved. No reuse allowed without permission.

792 bridge breakage in TREX1-null cells. Right: local fragmentation of the bridge
793 chromosome, with chromosome rearrangements (green arcs and orange lines) due to end-
794 joining of the resulting fragments.

795 **Figure 5. The Tandem Short Template (TST) jump rearrangement signature and aberrant**
796 **DNA replication within broken chromosome bridges.**

797 (A) Extreme breakpoint clustering near the site of chromosome bridge breakage. Copy number
798 (1-Mb bins, gray dots) and rearrangements (black curves and magenta lines) are shown as
799 in Fig. 3 for daughter cell (a) of the T-1 sample. Copy-number segmentation based on the
800 250-kb bin-level analysis (see Methods) is shown (bottom, black line). Uppermost
801 ("rainfall") plot shows the distance between adjacent breakpoints ($\log_{10}$ scale); clustering
802 of breakpoints is indicated from marked drops in inter-breakpoint distance (colored lines
803 correspond to rearrangement hotspots in panel B).

804 (B) Features of the TST jump signature. Top: One chain of short insertions, colored according
805 to their respective hotspot origin. The origin of each insertion in this chain is labeled in the
806 hotspot plot below, showing its order in the template chain (i, ii, iii, etc.). Bottom left: The
807 chain of insertions depicted above is shown as thick black lines, and other chains are thin
808 black lines. Magenta line shows a short insertion derived from Chr11. Bottom right: Each
809 hotspot (A-F) spans 1-2 kb and contains 4-8 short insertions (8-16 break ends); numbers
810 indicate the position of each hotspot on the reference genome. The TST insertions (not
811 drawn true-to-scale) within each hotspot often display partial overlap and form multiple
812 chains. Filled shapes: TST insertions in the single, long chain shown above. Unfilled
813 shapes: other TST insertions involved in different chains. Shapes open on one side

represent the start or end of chains, where only one segment boundary could be determined via SV analysis.

(C) Cytological observation of under-replication of chromatin in bridges. Cells with intact (top) or broken (bottom) chromosome bridges were pulse-labeled in S phase with EdU. Bridges, marked by cyan arrowheads, were visualized by staining for LAP2. Insets (magenta boxes) show the broken bridge stub.

(D) Example of interphase under-replication of DNA in bridges detected by single-cell sequencing. Cells were isolated after a Look-Seq experiment (Fig. 3A). Shown are copy number plots for the bridge haplotype (black dots) and the control, non-bridge haplotype (gray dots). Gray shading: region of under-replication of bridge haplotype. The mean copy number in this 20-Mb region (grey rectangle) for the bridge haplotype, 1.56, is lower than the expected gain (CN = 2) for this region. Partial retention of that haplotype in the sister cell (median CN of bridge haplotype = 0.05) does not explain the extent of "missing" DNA.

Figure 6. The Tandem Short Template (TST) jump rearrangement signature in primary clones from bridged cells and in a primary tumor sample.

(A) The TST jump signature is observed in bulk sequencing of the progeny of a single cell after bridge breakage. Top: DNA copy number of the bridge chromosome (Chr4) is shown as gray dots (250-kb bins). Long-range rearrangements (distance between breakpoints > 1Mb) on Chr4 are shown as black or colored curves. Three chains of complex rearrangements (similar to the chain illustrated in Fig. 5B), each consisting of 8-14 short templates originating from 11 breakpoint hotspots, are shown with blue, green, and red curves. Black curves indicate rearrangements not obviously linked in chains. Bottom: the chains of insertions are shown schematically, where templated insertions (gray boxes with black

837 outline) are connected as shown by blue, green, or red lines in an expanded view for each
838 breakpoint cluster (≤10-kb window in each region). Grey vertical lines are axis breaks
839 indicating distances larger than 10 kb.
840 (B) TST jump signature in a renal cell carcinoma sample. As in (A), upper plot shows copy
841 number (gray dots: 10-kb bins) and rearrangements (black lines) for the region of
842 unbalanced translocation between Chr3 and Chr5. Schematic below depicts one chain of
843 templated insertions from long-read sequencing data, in an expanded view for each
844 breakpoint cluster (3- to 10-kb windows in the hotspot regions labeled A-E).
845 (C) Chains of short insertions identified in bridged cells and in a primary tumor sample exhibit
846 a similar fragment size distribution. Histograms show the size distribution for chained short
847 insertions from single-cell sequencing of a daughter cell after bridge breakage (left; data
848 from Fig. 5B), from bulk sequencing of progeny derived from a single cell after bridge
849 breakage (center; data from panel A), and from long-read sequencing data from the renal
850 cell carcinoma sample (right; data from panel B).

851 **Figure 7. Aberrant DNA replication and extensive DNA damage on bridge DNA after mitotic**
852 **entry.**
853 (A) Correlative live-cell/fixed-cell imaging was used to monitor broken bridge chromosomes
854 entering the next mitosis. Left: schematic of the experiment. Right: example images show
855 cells with broken bridges in G2 arrest and after release into mitosis, as well as a control
856 mitotic cell that did not have a bridge in the prior interphase. Cyan arrowheads: bridge
857 chromosome.
858 (B) Quantification from (A).

(C) Images showing correlation of DNA damage (γ-H2AX) with RPA accumulation and active DNA replication (EdU). Cyan arrowheads: bridge chromosome.

(D) Representative time-lapse images showing a burst of mitotic DNA replication specifically on a chromosome from a broken bridge. Mitotic replication was visualized by GFP-RPA2; bridge with SNAP-BAF. During mitosis, high activity of vaccinia related kinase (VRK) inactivates DNA binding by BAF (10 to 25 min). Orange arrowheads indicate the broken bridge chromosome. Note that an unrelated interphase cell migrates through the bottom of the field of view in several frames (10 to 35 min). Confocal imaging was performed with a 40× objective, 7 z-slices at 1-μm spacing, acquired every 5 min.

Figure 8. Centromere inactivation on chromosomes within bridges leads to frequent micronucleation.

(A) Frequent micronucleation in the second generation after bridge formation. Left: schematic of the live-cell imaging experiment. A cell divides, forming a bridge between two daughter cells in the first generation. After the bridge breaks, the daughter cells with broken bridge stubs divide, generating four “grand-daughter” cells in the second generation. The frequency of micronucleation in second generation cells was measured in control cells that did not have a bridge in the first generation (No bridge) as compared to cells that did (Bridge). Right: quantification of data from the experiment.

(B) Micronuclei derived from a bridge chromosome usually retain their centromeres. Left: fluorescence in situ hybridization (FISH) to detect whole-chromosome 4 (Chr4 paint, red) and Chr4 centromere (CEN4, green) in first- and second-generation cells after CRISPR-mediated Chr4 bridge formation. Right: quantification of CEN4 status of Chr4-containing MN in second-generation cells.

(C) Centromere defects explain the high rate of micronucleation after chromosome bridge formation. Left: representative images showing CENP-A-Halo labeling (green) and anti-centromere FISH (red) to assess centromere integrity of chromosomes in micronuclei (second-generation cells, as in (A)). Cyan arrowheads indicate the location of the centromere (FISH signal) in micronuclei. Right: quantification of CENP-A-Halo levels at centromeres in micronuclei (MN), relative to those in primary nuclei (PN), $p < 0.0001$ (paired *t*-test). Bridges were induced in the first generation by transient TRF2-DN expression. Only centromere DNA-containing micronuclei were analyzed.

Figure 9. Micronuclei develop extensive DNA damage associated with a burst of mitotic DNA synthesis, which promotes chromothripsis.

(A) Modest DNA damage is associated with defective replication in intact micronuclei of G2 cells. Top: schematic of the experiment. Micronuclei were induced by a nocodazole washout procedure (*17*), and EdU was added in G1 to visualize all DNA replication during the following S phase. Cells were then fixed in G2 (22 hours after mitosis). Where indicated, small-molecule inhibitors of Dbf4-dependent kinase (PHA-767491) or cyclin-dependent kinase (flavopiridol) were also added in G1 to block the initiation of DNA replication. Bottom: example images show intact micronuclei (assessed by RFP-NLS), with counter-staining to relate the extent of DNA replication (EdU) to the amount of DNA damage (γ-H2AX). Robust γ-H2AX signal was correlated with diminished EdU signal and was blocked by the DDK or CDK inhibitors.

(B) Quantification of (A) showing DNA damage in micronuclei with poor DNA replication. Left: DNA damage in intact micronuclei (ratio of γ-H2AX intensity in the micronucleus relative to the primary nucleus) relative to replication proficiency (EdU ratio). Dashed red

bioRxiv preprint doi: https://doi.org/10.1101/835058; this version posted November 7, 2019. The copyright holder for this preprint (which was not peer-reviewed) is the author/funder, who has granted bioRxiv a license to display the preprint in perpetuity. All rights reserved. No reuse allowed without permission.

905 line indicates the threshold (three standard deviations above the mean intensity for primary
906 nuclei) above which micronuclei were scored as positive for DNA damage. Right:
907 compared to control, CDKi (p = 0.01) or DDKi (p = 0.0008) prevents DNA damage in
908 intact micronuclei; p-values determined by Mann-Whitney test.
909 (C) Complex rearrangement of a chromosome from an intact micronucleus in a G2 cell. The
910 chromosome from the micronucleus (Chr2) is under-replicated and was identified by its
911 odd-numbered copy number state. The mis-segregation generating this micronucleus
912 resulted in a diploid cell with an extra copy of Chr2 from the micronucleus (2N+1) (*17*).
913 Black dots: 1-Mb bins for the haplotype of the micronuclear chromosome, which together
914 with the fully replicated copy of Chr2 haplotype in the primary nucleus, leads to black copy
915 number of ~3. Gray dots: the other Chr2 haplotype, which is also in the primary nucleus
916 and present at a copy number of 2. n = 1 of 10 cells examined; the remaining 9 G2
917 micronucleated cells did not exhibit rearrangement of the micronucleated chromosome.
918 (D) Mitotic DNA replication and DNA damage (synchronized fixed cells), similar to Fig. 7C,
919 for cells induced to form micronuclei by nocodazole washout. Cyan arrowheads:
920 micronucleated chromosome.
921 (E) Parallel experiments as in Fig. 7A-B, for cells with intact micronuclei that were released
922 into mitosis. To avoid confounding DNA damage from interphase nuclear envelope
923 rupture, only cells with intact micronuclei (RFP-NLS) were analyzed. Cyan arrowheads:
924 micronucleated chromosome.
925 (F) Quantification from (E). Levels of DNA damage on the micronucleated chromosome
926 increased ~10-fold in mitotic cells compared to G2 cells ($p < 0.0001$, left plot), concomitant

with abrupt initiation of mitotic DNA synthesis as indicated by RPA1 accumulation ($p <$ 0.0001, right plot); *p*-values calculated by Mann-Whitney test.

(G) Complex rearrangement of a chromosome from an intact micronucleus after passing through mitosis. Copy number and rearrangements are shown for the micronucleated chromosome (one haplotype of Chr2), identified by its odd copy number as described in (C). 8 of 9 daughter pairs examined evidenced complex rearrangements on the micronucleated chromosome.

Figure 10. Extensive genetic heterogeneity after chromosome bridge formation.

(A) Multiple co-existing subclones in a population derived from a cell with a broken chromosome bridge (Chr4, see Fig. S1). Top: DNA copy number of the two Chr4 homologs (red and blue dots, 25-kb bins) from bulk DNA sequencing of Primary Clone 2a. Non-integer copy number indicates the presence of multiple subclones with different copy number states.

(B) Heatmap of DNA copy number for Homolog A on the p-arm of Chr4 (0-50 Mb) in ~800 single cells, where each row represents one cell. Different subclonal populations can be identified with copy number profiles consistent with those seen in single cell-derived subclones shown in (C).

(C) DNA copy number of Chr4p Homolog A (red dots, 25-kb bins) in three subclones grown from single cells isolated from Primary Clone 2a. The copy number state is shown schematically above each plot. The copy number change point shared across all subclones (dashed orange line) is inferred to have resulted from breakage of the Chr4 bridge chromosome in the first generation. Other copy number changes that were shared only among a subset of subclones (dashed purple line), or were private to individual

subclones (dashed cyan lines), suggest that these more complex patterns arose during later generations downstream of the initial bridge breakage event.

(D) Evidence of ongoing chromosomal instability in Chr4 bridge primary clones indicated by copy number variations across subclones. Top: Bulk DNA copy number of Homolog A (red) and Homolog B (blue) on Chr4p (0-50Mb) in Primary Clone 1a. Bottom: Copy number profiles of each homolog in single-cell derived subclones. The first profile of Homolog A was observed together with each of the first eight profiles of Homolog B, as shown by the thick black lines. Similarly, the next five profiles of Homolog A were each observed together with the ninth profile of Homolog B. The last profiles of Homologs A and B were observed together (two independent subclones). Copy number breakpoints on Homolog A that are shared among all subclones are indicated by vertical dashed black lines. Variations in Homolog A range from focal copy number changes (red arrows), including focal amplifications, to near-complete arm loss (last profile). Profiles of Homolog B show different degrees of terminal loss, a pattern that suggests ongoing instability affecting this chromosome. This is supported by the observation that many of these Homolog B profiles were present at a low clonal fraction (i.e. observed in only one subclone). Therefore, this progressive terminal loss pattern might represent a snapshot of ongoing evolution that eventually results in complete loss of the chromosome arm.

ACKNOWLEDGEMENTS

We would like to thank M. Bao, P. Campbell, M. Kwon, J. Lee, S. Liu, M. Meyerson, J. Walter, and K. Xie for comments on the manuscript; I. Cheeseman, Maciejowski and T. de Lange for reagents; P. Campbell, J. Maciejowski and T. de Lange for sharing unpublished results. N.T.U.

973 was an HHMI Fellow of the Damon Runyon Cancer Institute and is supported by the Claudia
974 Adams Barr Program for Innovative Cancer Research. T.M. is supported by Cancer Research UK
975 and the Royal College of Surgeons (C63474/A27176). C.-Z.Z. is supported by an NCI career
976 transition award (K22CA216319). C.-Z.Z and L.S. are supported by an NCI Cancer Moonshot
977 award (1R33CA225344.). R.T. and H.F.A. are supported by the Harvard University Milton Fund.
978 A.S. is supported by an NCI Mentored Clinical Scientist Research Career Development
979 Award (K08CA208008) and a Burroughs-Wellcome Career Award for Medical Scientists
980 (CAMS). D.P. is a HHMI investigator and is supported by NIH grant GM083299, a Research
981 Investigator Award from the Lustgarten Foundation, and an award from the G. Harold and Leila
982 Y. Mathers Charitable Foundation.

983

984 ## AUTHOR CONTRIBUTIONS

985 D.P., N.T.U., and C.-Z.Z. conceived the project. D.P. and N.T.U. designed the biological
986 experiments, which were performed by A.M.C., L.D.L. and N.T.U. D.P., N.T.U., and C.-Z.Z.
987 designed the sequencing experiments, which were performed by L.S. and N.T.U. C.-Z.Z. designed
988 and performed the analysis of single-cell and bulk sequencing data of RPE-1 samples, with help
989 from L.J.B. The low-pass single-cell CNV analysis was performed by R.T. and H.F.A. T.J.M.,
990 and K.J. contributed the data and analysis in Fig. 5D. A.S. contributed the data in Figs. 7C and
991 7G, and to early experiments on the project. D.P. and N.T.U. wrote the manuscript with edits from
992 other authors.

993

994

SUPPLEMENTAL MATERIALS

Materials and Methods

Table S1.

Figures S1-S20

Movies S1-S16

References 84-95

REFERENCES

1. P. J. Campbell, G. Getz, J. M. Stuart, J. O. Korbel, L. D. Stein, Pan-cancer analysis of whole genomes. *BioRxiv*, (2017).
2. T. Fujiwara *et al.*, Cytokinesis failure generating tetraploids promotes tumorigenesis in p53-null cells. *Nature* **437**, 1043-1047 (2005).
3. M. L. Leibowitz, C. Z. Zhang, D. Pellman, Chromothripsis: A New Mechanism for Rapid Karyotype Evolution. *Annu Rev Genet* **49**, 183-211 (2015).
4. P. Ly, D. W. Cleveland, Rebuilding Chromosomes After Catastrophe: Emerging Mechanisms of Chromothripsis. *Trends Cell Biol* **27**, 917-930 (2017).
5. P. J. Stephens *et al.*, Massive genomic rearrangement acquired in a single catastrophic event during cancer development. *Cell* **144**, 27-40 (2011).
6. S. Turajlic, A. Sottoriva, T. Graham, C. Swanton, Resolving genetic heterogeneity in cancer. *Nat Rev Genet* **20**, 404-416 (2019).
7. S. M. A. Lens, R. H. Medema, Cytokinesis defects and cancer. *Nat Rev Cancer* **19**, 32-45 (2019).
8. N. J. Ganem, S. A. Godinho, D. Pellman, A mechanism linking extra centrosomes to chromosomal instability. *Nature* **460**, 278-282 (2009).
9. M. Kwon *et al.*, Mechanisms to suppress multipolar divisions in cancer cells with extra centrosomes. *Genes Dev* **22**, 2189-2203 (2008).
10. S. P. R *et al.*, Profiling DNA damage response following mitotic perturbations. *Nat Commun* **7**, 13887 (2016).
11. D. Cimini *et al.*, Merotelic kinetochore orientation is a major mechanism of aneuploidy in mitotic mammalian tissue cells. *J Cell Biol* **153**, 517-527 (2001).
12. P. Liu *et al.*, Chromosome catastrophes involve replication mechanisms generating complex genomic rearrangements. *Cell* **146**, 889-903 (2011).

13. F. Notta *et al.*, A renewed model of pancreatic cancer evolution based on genomic rearrangement patterns. *Nature* **538**, 378-382 (2016).
14. K. Crasta *et al.*, DNA breaks and chromosome pulverization from errors in mitosis. *Nature* **482**, 53-58 (2012).
15. P. Ly *et al.*, Selective Y centromere inactivation triggers chromosome shattering in micronuclei and repair by non-homologous end joining. *Nat Cell Biol* **19**, 68-75 (2017).
16. P. N. Rao, R. T. Johnson, Premature Chromosome Condensation. *Academic Press*, (1982).
17. C. Z. Zhang *et al.*, Chromothripsis from DNA damage in micronuclei. *Nature* **522**, 179-184 (2015).
18. E. M. Hatch, A. H. Fischer, T. J. Deerinck, M. W. Hetzer, Catastrophic nuclear envelope collapse in cancer cell micronuclei. *Cell* **154**, 47-60 (2013).
19. S. Liu *et al.*, Nuclear envelope assembly defects link mitotic errors to chromothripsis. *Nature* **561**, 551-555 (2018).
20. J. Maciejowski, T. de Lange, Telomeres in cancer: tumour suppression and genome instability. *Nat Rev Mol Cell Biol* **18**, 175-186 (2017).
21. B. McClintock, The Stability of Broken Ends of Chromosomes in Zea Mays. *Genetics* **26**, 234-282 (1941).
22. N. Shimizu, K. Shingaki, Y. Kaneko-Sasaguri, T. Hashizume, T. Kanda, When, where and how the bridge breaks: anaphase bridge breakage plays a crucial role in gene amplification and HSR generation. *Exp Cell Res* **302**, 233-243 (2005).
23. Y. Li *et al.*, Constitutional and somatic rearrangement of chromosome 21 in acute lymphoblastic leukaemia. *Nature* **508**, 98-102 (2014).
24. J. G. Carlton, A. Caballe, M. Agromayor, M. Kloc, J. Martin-Serrano, ESCRT-III governs the Aurora B-mediated abscission checkpoint through CHMP4C. *Science* **336**, 220-225 (2012).
25. A. Janssen, M. van der Burg, K. Szuhai, G. J. Kops, R. H. Medema, Chromosome segregation errors as a cause of DNA damage and structural chromosome aberrations. *Science* **333**, 1895-1898 (2011).
26. J. Maciejowski, Y. Li, N. Bosco, P. J. Campbell, T. de Lange, Chromothripsis and Kataegis Induced by Telomere Crisis. *Cell* **163**, 1641-1654 (2015).
27. P. Steigemann *et al.*, Aurora B-mediated abscission checkpoint protects against tetraploidization. *Cell* **136**, 473-484 (2009).
28. B. van Steensel, A. Smogorzewska, T. de Lange, TRF2 protects human telomeres from end-to-end fusions. *Cell* **92**, 401-413 (1998).
29. T. A. Hartl, S. J. Sweeney, P. J. Knepler, G. Bosco, Condensin II resolves chromosomal associations to enable anaphase I segregation in Drosophila male meiosis. *PLoS Genet* **4**, e1000228 (2008).
30. C. F. Nielsen *et al.*, PICH promotes sister chromatid disjunction and co-operates with topoisomerase II in mitosis. *Nat Commun* **6**, 8962 (2015).
31. M. Thery, Micropatterning as a tool to decipher cell morphogenesis and functions. *J Cell Sci* **123**, 4201-4213 (2010).
32. B. J. Belin, L. M. Goins, R. D. Mullins, Comparative analysis of tools for live cell imaging of actin network architecture. *Bioarchitecture* **4**, 189-202 (2014).
33. Y. Ren *et al.*, Mechanosensing through cooperative interactions between myosin II and the actin crosslinker cortexillin I. *Curr Biol* **19**, 1421-1428 (2009).

1075 34. S. L. Gupton, C. M. Waterman-Storer, Spatiotemporal feedback between actomyosin and
1076 focal-adhesion systems optimizes rapid cell migration. *Cell* **125**, 1361-1374 (2006).
1077 35. V. G. Brunton, I. R. MacPherson, M. C. Frame, Cell adhesion receptors, tyrosine kinases
1078 and actin modulators: a complex three-way circuitry. *Biochim Biophys Acta* **1692**, 121-
1079 144 (2004).
1080 36. S. Miyamoto, B. Z. Katz, R. M. Lafrenie, K. M. Yamada, Fibronectin and integrins in
1081 cell adhesion, signaling, and morphogenesis. *Ann N Y Acad Sci* **857**, 119-129 (1998).
1082 37. A. Saez, A. Buguin, P. Silberzan, B. Ladoux, Is the mechanical activity of epithelial cells
1083 controlled by deformations or forces? *Biophys J* **89**, L52-54 (2005).
1084 38. M. Crisp *et al.*, Coupling of the nucleus and cytoplasm: role of the LINC complex. *J Cell*
1085 *Biol* **172**, 41-53 (2006).
1086 39. D. A. Starr, H. N. Fridolfsson, Interactions between nuclei and the cytoskeleton are
1087 mediated by SUN-KASH nuclear-envelope bridges. *Annu Rev Cell Dev Biol* **26**, 421-444
1088 (2010).
1089 40. T. Takaki *et al.*, Actomyosin drives cancer cell nuclear dysmorphia and threatens genome
1090 stability. *Nat Commun* **8**, 16013 (2017).
1091 41. A. Smogorzewska, J. Karlseder, H. Holtgreve-Grez, A. Jauch, T. de Lange, DNA ligase
1092 IV-dependent NHEJ of deprotected mammalian telomeres in G1 and G2. *Curr Biol* **12**,
1093 1635-1644 (2002).
1094 42. Y. Li *et al.*, Patterns of structural variations in human cancer. *BioRxiv*, (2017).
1095 43. S. Nik-Zainal *et al.*, Mutational processes molding the genomes of 21 breast cancers. *Cell*
1096 **149**, 979-993 (2012).
1097 44. S. A. Roberts *et al.*, Clustered mutations in yeast and in human cancers can arise from
1098 damaged long single-strand DNA regions. *Mol Cell* **46**, 424-435 (2012).
1099 45. J. O. Korbel, P. J. Campbell, Criteria for inference of chromothripsis in cancer genomes.
1100 *Cell* **152**, 1226-1236 (2013).
1101 46. F. Zhang *et al.*, The DNA replication FoSTeS/MMBIR mechanism can generate
1102 genomic, genic and exonic complex rearrangements in humans. *Nat Genet* **41**, 849-853
1103 (2009).
1104 47. R. P. Anand *et al.*, Chromosome rearrangements via template switching between
1105 diverged repeated sequences. *Genes Dev* **28**, 2394-2406 (2014).
1106 48. T. J. Mitchell *et al.*, Timing the Landmark Events in the Evolution of Clear Cell Renal
1107 Cell Cancer: TRACERx Renal. *Cell* **173**, 611-623 e617 (2018).
1108 49. L. Costantino *et al.*, Break-induced replication repair of damaged forks induces genomic
1109 duplications in human cells. *Science* **343**, 88-91 (2014).
1110 50. J. Kramara, B. Osia, A. Malkova, Break-Induced Replication: The Where, The Why, and
1111 The How. *Trends Genet* **34**, 518-531 (2018).
1112 51. L. Deng *et al.*, Mitotic CDK Promotes Replisome Disassembly, Fork Breakage, and
1113 Complex DNA Rearrangements. *Mol Cell* **73**, 915-929 e916 (2019).
1114 52. R. Bhowmick, I. D. Hickson, The "enemies within": regions of the genome that are
1115 inherently difficult to replicate. *F1000Res* **6**, 666 (2017).
1116 53. M. Soto, I. Garcia-Santisteban, L. Krenning, R. H. Medema, J. A. Raaijmakers,
1117 Chromosomes trapped in micronuclei are liable to segregation errors. *J Cell Sci* **131**,
1118 (2018).
1119 54. D. Fachinetti *et al.*, A two-step mechanism for epigenetic specification of centromere
1120 identity and function. *Nat Cell Biol* **15**, 1056-1066 (2013).

55. S. Z. Swartz *et al.*, Quiescent Cells Actively Replenish CENP-A Nucleosomes to Maintain Centromere Identity and Proliferative Potential. *Dev Cell* **51**, 35-48 e37 (2019).
56. D. W. Garsed *et al.*, The architecture and evolution of cancer neochromosomes. *Cancer Cell* **26**, 653-667 (2014).
57. K. M. Stimpson *et al.*, Telomere disruption results in non-random formation of de novo dicentric chromosomes involving acrocentric human chromosomes. *PLoS Genet* **6**, (2010).
58. D. K. Butler, Ribosomal DNA is a site of chromosome breakage in aneuploid strains of Neurospora. *Genetics* **131**, 581-592 (1992).
59. B. McClintock, The Behavior in Successive Nuclear Divisions of a Chromosome Broken at Meiosis. *Proc Natl Acad Sci U S A* **25**, 405-416 (1939).
60. B. McClintock, Spontaneous alterations in chromosome size and form in *Zea mays*. *Cold Spring Harb Symp Quant Biol* **9**, 72-81 (1941).
61. D. Choquet, D. P. Felsenfeld, M. P. Sheetz, Extracellular matrix rigidity causes strengthening of integrin-cytoskeleton linkages. *Cell* **88**, 39-48 (1997).
62. E. S. Schiffhauer *et al.*, Mechanoaccumulative Elements of the Mammalian Actin Cytoskeleton. *Curr Biol* **26**, 1473-1479 (2016).
63. D. Bensimon, A. J. Simon, V. V. Croquette, A. Bensimon, Stretching DNA with a receding meniscus: Experiments and models. *Phys Rev Lett* **74**, 4754-4757 (1995).
64. M. Grandbois, M. Beyer, M. Rief, H. Clausen-Schaumann, H. E. Gaub, How strong is a covalent bond? *Science* **283**, 1727-1730 (1999).
65. N. Q. Balaban *et al.*, Force and focal adhesion assembly: a close relationship studied using elastic micropatterned substrates. *Nat Cell Biol* **3**, 466-472 (2001).
66. O. du Roure *et al.*, Force mapping in epithelial cell migration. *Proc Natl Acad Sci U S A* **102**, 2390-2395 (2005).
67. J. L. Tan *et al.*, Cells lying on a bed of microneedles: an approach to isolate mechanical force. *Proc Natl Acad Sci U S A* **100**, 1484-1489 (2003).
68. M. L. Bennink *et al.*, Unfolding individual nucleosomes by stretching single chromatin fibers with optical tweezers. *Nat Struct Biol* **8**, 606-610 (2001).
69. C. M. Carvalho, J. R. Lupski, Mechanisms underlying structural variant formation in genomic disorders. *Nat Rev Genet* **17**, 224-238 (2016).
70. J. A. Wala *et al.*, SvABA: genome-wide detection of structural variants and indels by local assembly. *Genome Res* **28**, 581-591 (2018).
71. J. J. Lee *et al.*, Tracing Oncogene Rearrangements in the Mutational History of Lung Adenocarcinoma. *Cell* **177**, 1842-1857 e1821 (2019).
72. D. Zink, A. H. Fischer, J. A. Nickerson, Nuclear structure in cancer cells. *Nat Rev Cancer* **4**, 677-687 (2004).
73. T. A. Prokhorova, K. Mowrer, C. H. Gilbert, J. C. Walter, DNA replication of mitotic chromatin in Xenopus egg extracts. *Proc Natl Acad Sci U S A* **100**, 13241-13246 (2003).
74. S. C. West *et al.*, Resolution of Recombination Intermediates: Mechanisms and Regulation. *Cold Spring Harb Symp Quant Biol* **80**, 103-109 (2015).
75. S. Priego Moreno, R. M. Jones, D. Poovathumkadavil, S. Scaramuzza, A. Gambus, Mitotic replisome disassembly depends on TRAIP ubiquitin ligase activity. *Life Sci Alliance* **2**, (2019).
76. P. Ly *et al.*, Chromosome segregation errors generate a diverse spectrum of simple and complex genomic rearrangements. *Nat Genet* **51**, 705-715 (2019).

77. S. Henikoff, T. Furuyama, Epigenetic inheritance of centromeres. *Cold Spring Harb Symp Quant Biol* **75**, 51-60 (2010).
78. Y. Nechemia-Arbely, D. Fachinetti, D. W. Cleveland, Replicating centromeric chromatin: spatial and temporal control of CENP-A assembly. *Exp Cell Res* **318**, 1353-1360 (2012).
79. L. R. Gehlen *et al.*, Nuclear geometry and rapid mitosis ensure asymmetric episome segregation in yeast. *Curr Biol* **21**, 25-33 (2011).
80. D. Deckbar *et al.*, Chromosome breakage after G2 checkpoint release. *J Cell Biol* **176**, 749-755 (2007).
81. J. van den Berg *et al.*, A limited number of double-strand DNA breaks is sufficient to delay cell cycle progression. *Nucleic Acids Res* **46**, 10132-10144 (2018).
82. C. Ribeyre, D. Shore, Regulation of telomere addition at DNA double-strand breaks. *Chromosoma* **122**, 159-173 (2013).
83. R. L. Dilley *et al.*, Break-induced telomere synthesis underlies alternative telomere maintenance. *Nature* **539**, 54-58 (2016).
84. K. L. McKinley, I. M. Cheeseman, Large-Scale Analysis of CRISPR/Cas9 Cell-Cycle Knockouts Reveals the Diversity of p53-Dependent Responses to Cell-Cycle Defects. *Dev Cell* **40**, 405-420 e402 (2017).
85. S. K. Wu *et al.*, Cortical F-actin stabilization generates apical-lateral patterns of junctional contractility that integrate cells into epithelia. *Nat Cell Biol* **16**, 167-178 (2014).
86. A. Chicas *et al.*, Dissecting the unique role of the retinoblastoma tumor suppressor during cellular senescence. *Cancer Cell* **17**, 376-387 (2010).
87. A. Montagnoli *et al.*, A Cdc7 kinase inhibitor restricts initiation of DNA replication and has antitumor activity. *Nat Chem Biol* **4**, 357-365 (2008).
88. A. Sakaue-Sawano *et al.*, Visualizing spatiotemporal dynamics of multicellular cell-cycle progression. *Cell* **132**, 487-498 (2008).
89. M. Lobrich, B. Rydberg, P. K. Cooper, Repair of x-ray-induced DNA double-strand breaks in specific Not I restriction fragments in human fibroblasts: joining of correct and incorrect ends. *Proc Natl Acad Sci U S A* **92**, 12050-12054 (1995).
90. K. H. Miga, C. Eisenhart, W. J. Kent, Utilizing mapping targets of sequences underrepresented in the reference assembly to reduce false positive alignments. *Nucleic Acids Res* **43**, e133 (2015).
91. C. Chen *et al.*, Single-cell whole-genome analyses by Linear Amplification via Transposon Insertion (LIANTI). *Science* **356**, 189-194 (2017).
92. R. W. Tourdot, C.-Z. Zhang, Whole Chromosome Haplotype Phasing from Long-Range Sequencing. *bioRxiv*, 629337 (2019).
93. M. D. Young *et al.*, Single-cell transcriptomes from human kidneys reveal the cellular identity of renal tumors. *Science* **361**, 594-599 (2018).
94. P. J. Campbell *et al.*, Identification of somatically acquired rearrangements in cancer using genome-wide massively parallel paired-end sequencing. *Nat Genet* **40**, 722-729 (2008).
95. H. Li, Minimap2: pairwise alignment for nucleotide sequences. *Bioinformatics* **34**, 3094-3100 (2018).

Figure 1

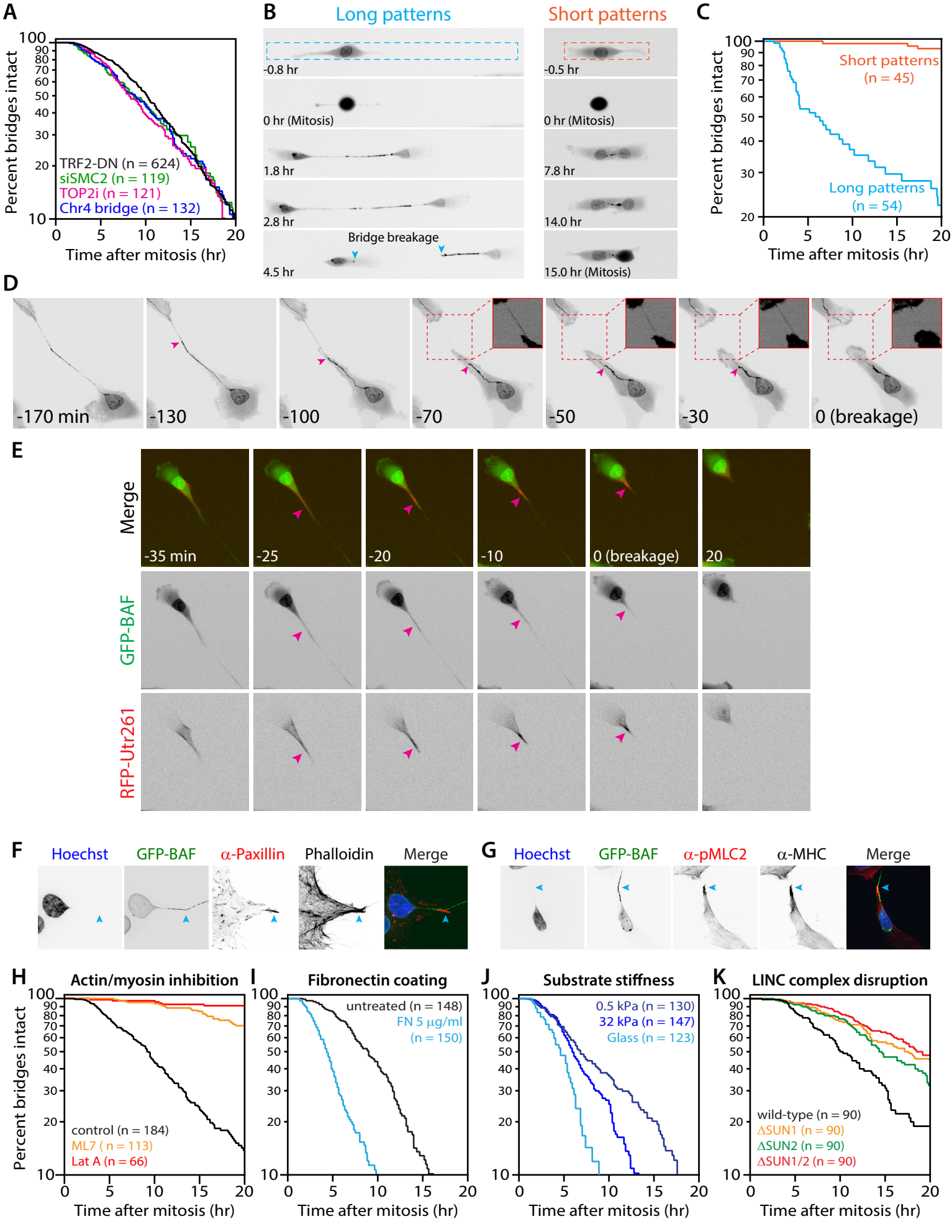

Figure 2

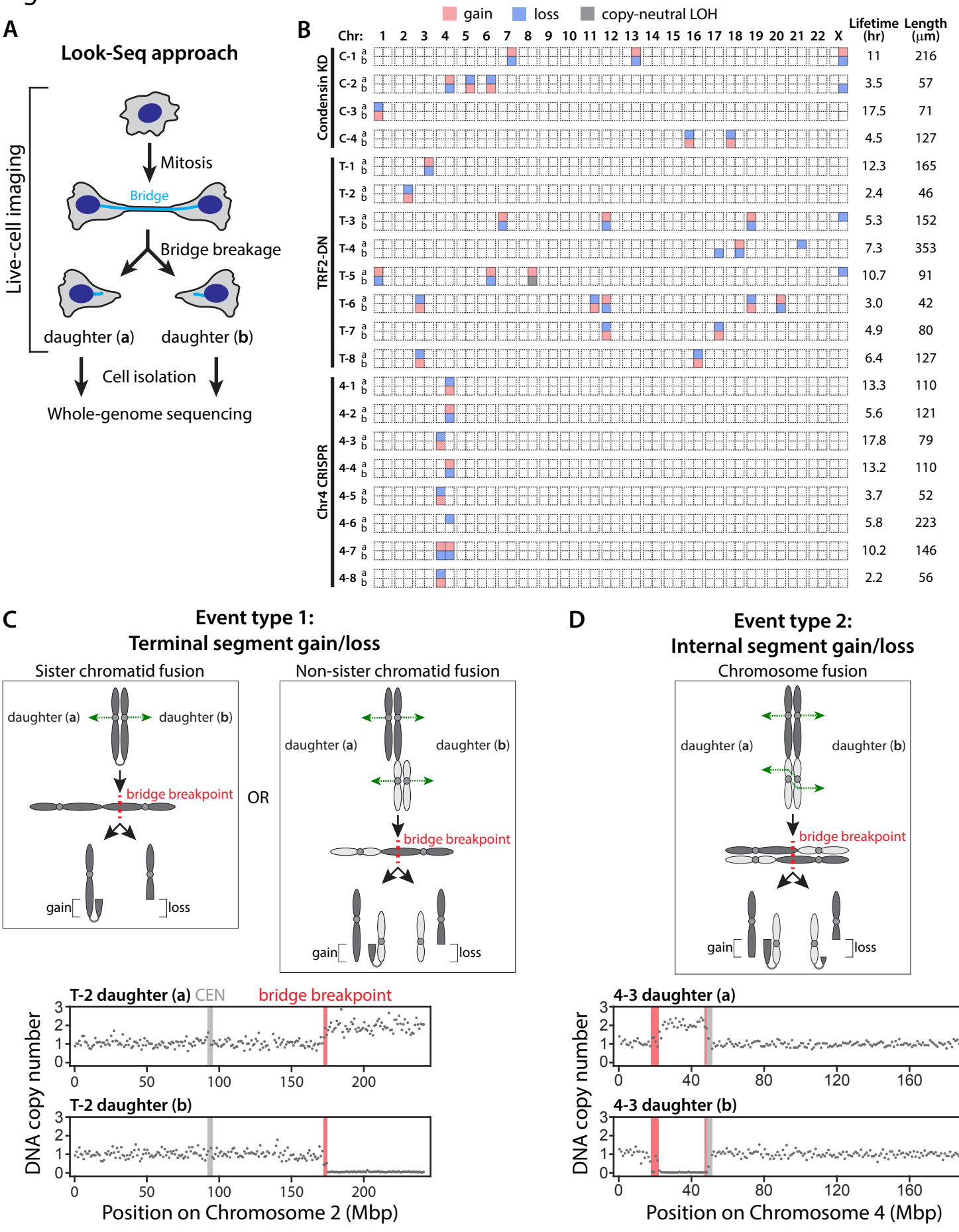

Figure 3

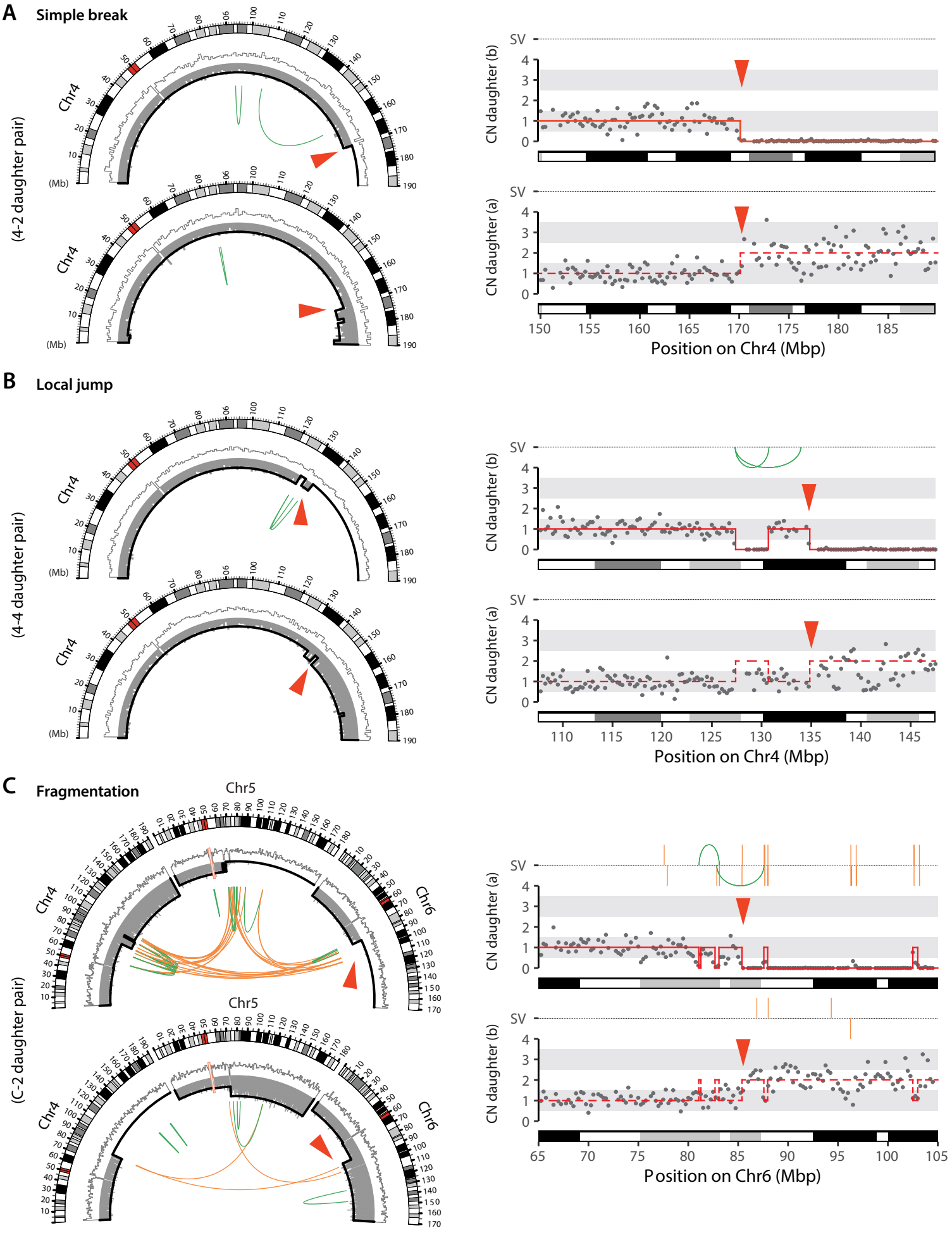

Figure 4

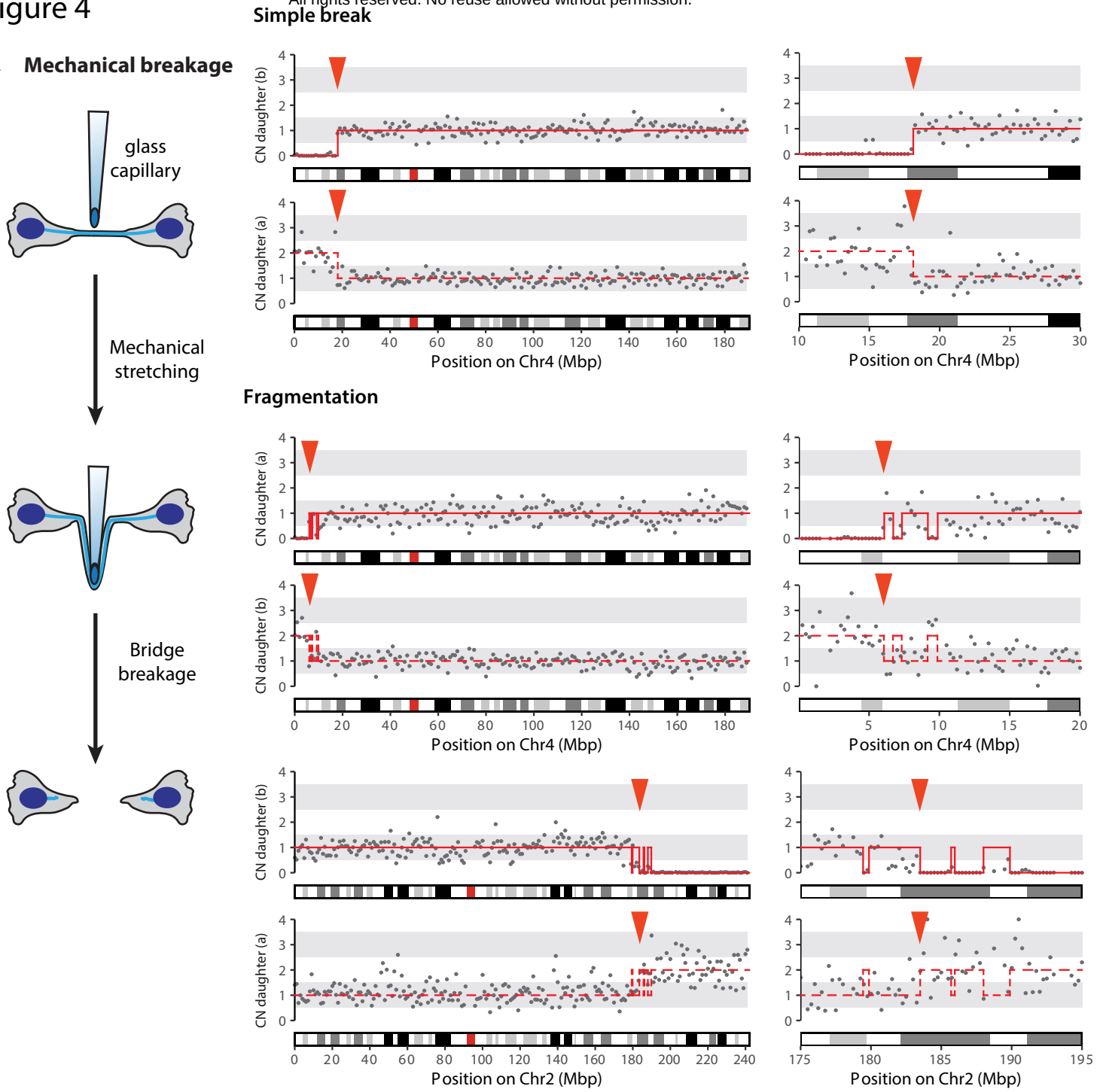

Figure 5

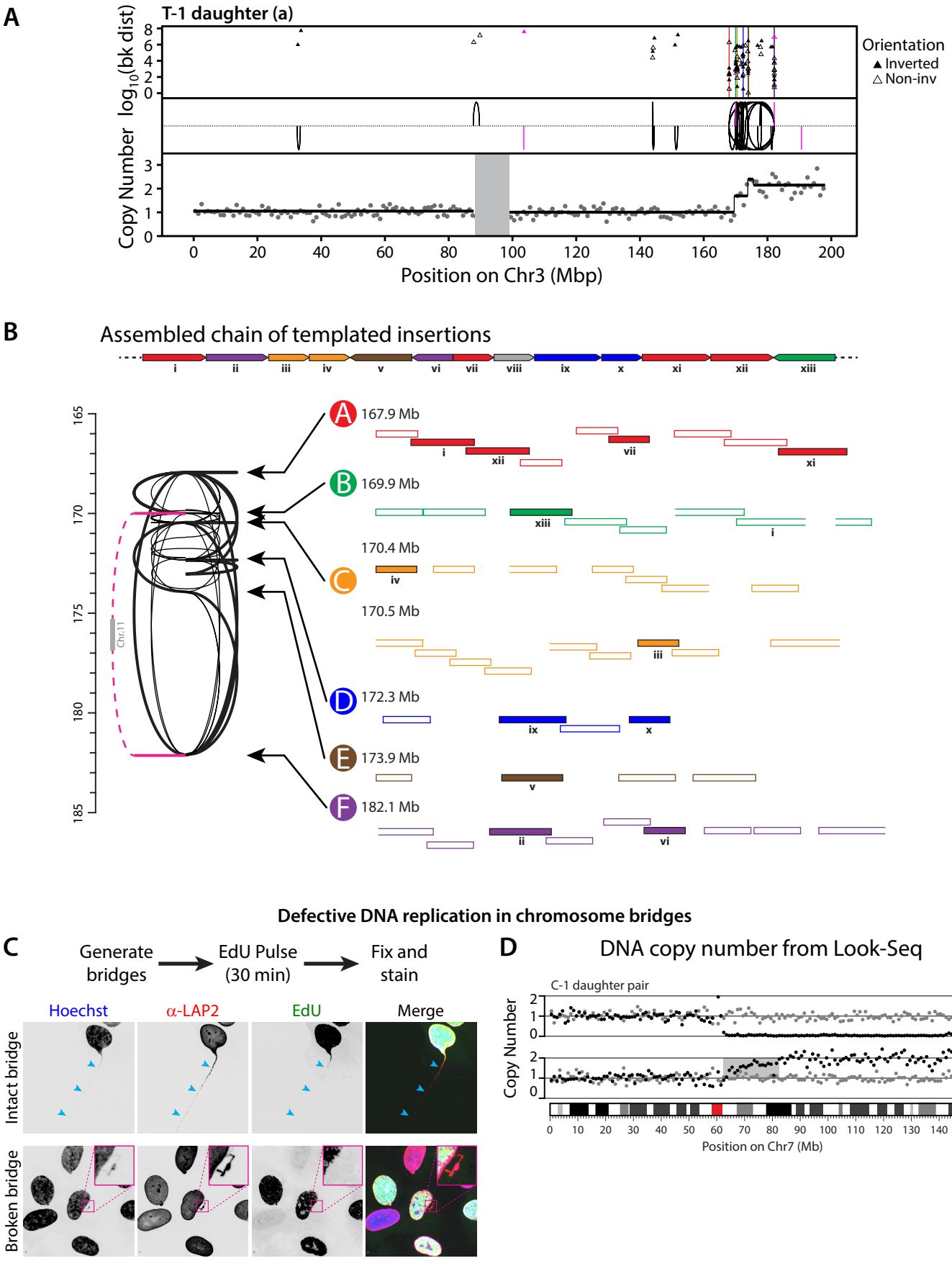

Figure 6

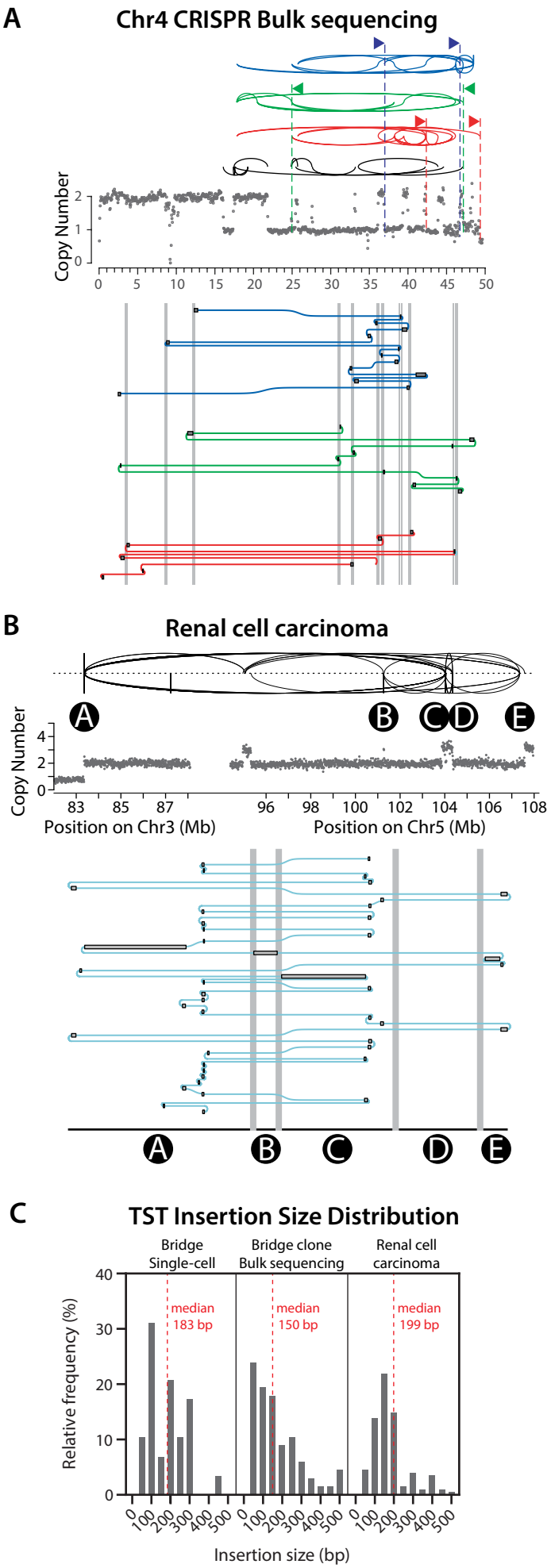

Figure 7

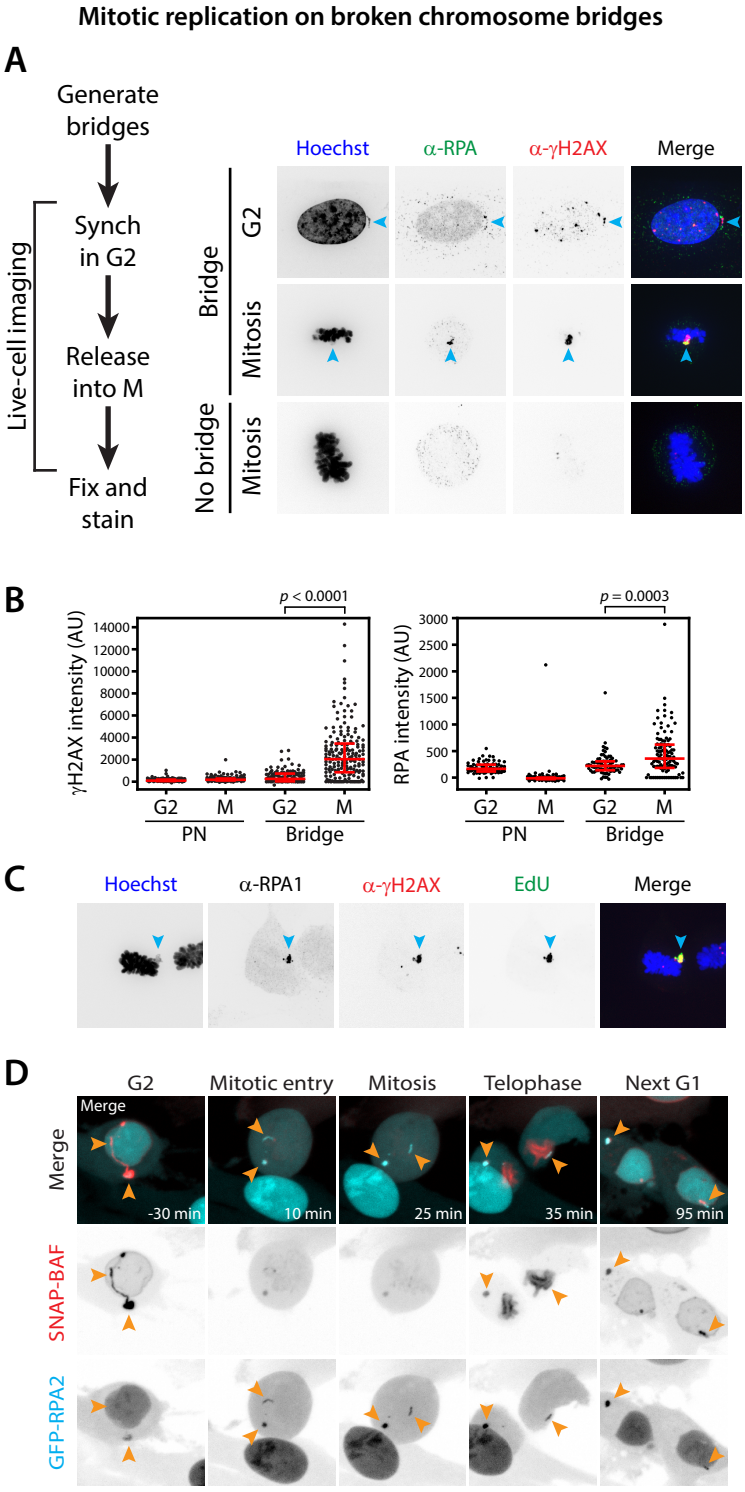

Figure 8

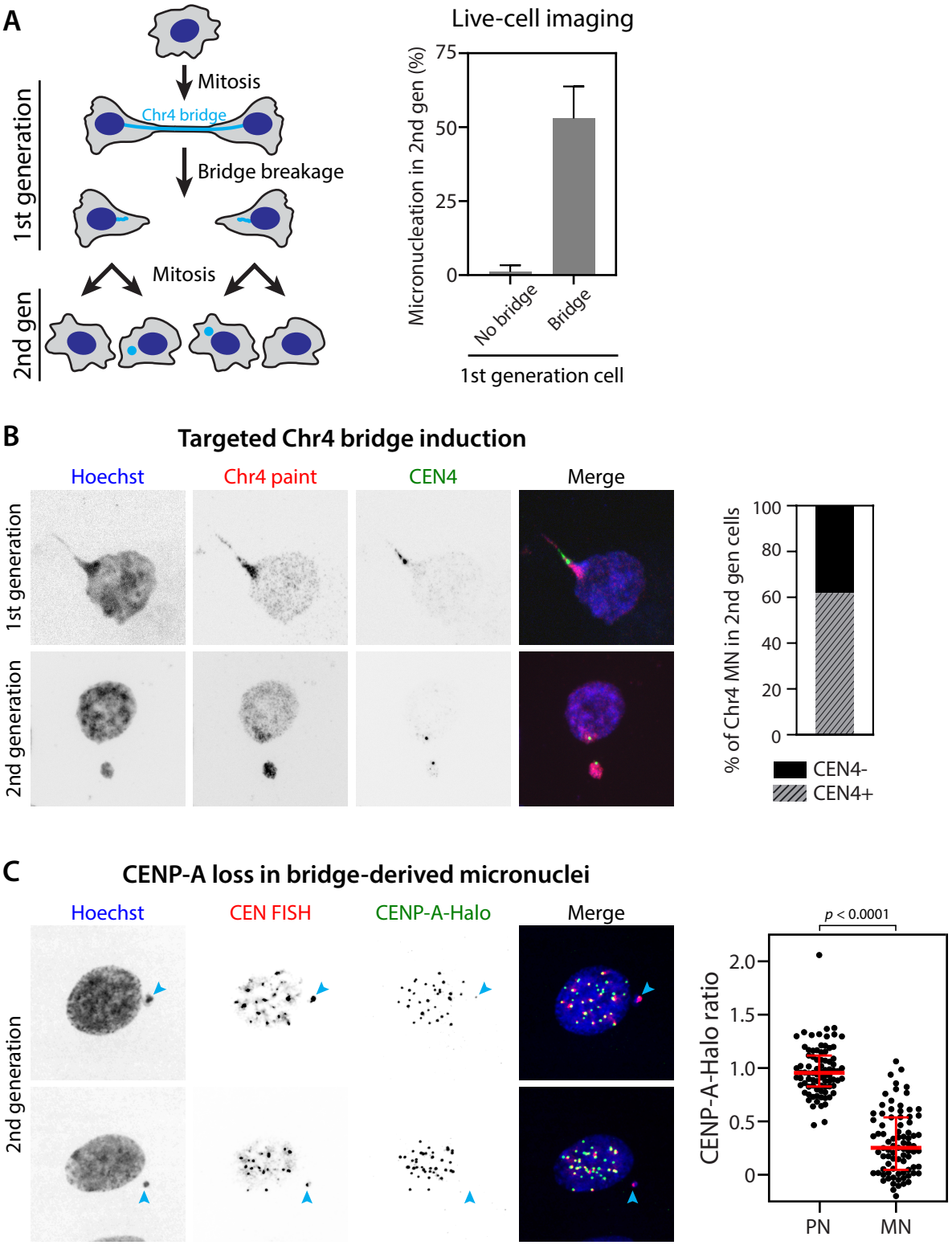

Figure 9

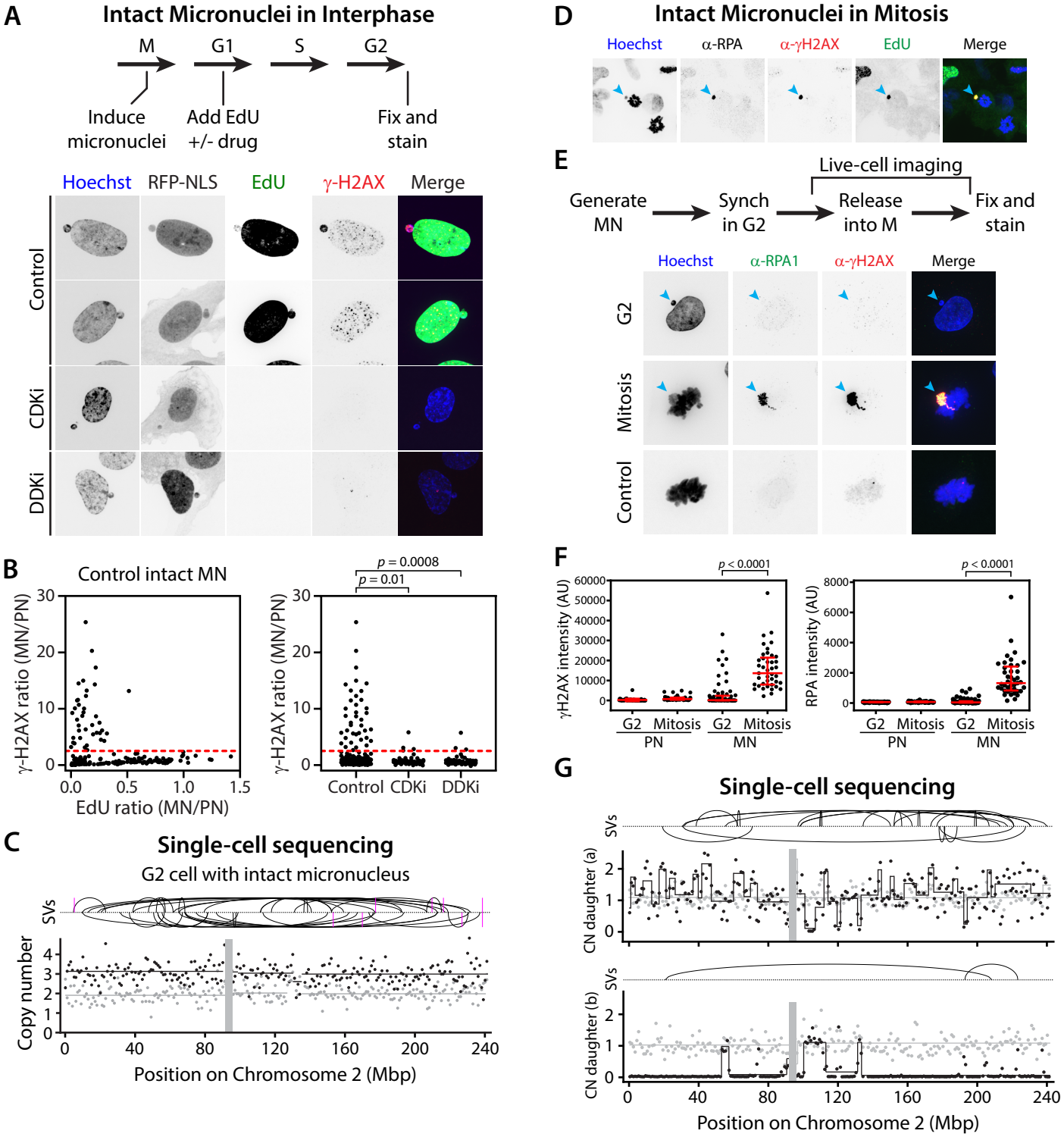

Figure 10